UNIVERSITY OF THESSALY

SCHOOL OF ENGINEERING

DEPARTMENT OF MECHANICAL ENGINEERING

STRUCTURAL ANALYSIS OF A STEEL FLOATING PLATFORM FOR THE SUPPORT OF A 10 MW WIND TURBINE

by

GEORGIOS PAPADOPOULOS

Mechanical Engineer, University of Thessaly, 2022

Submitted in partial fulfillment of the requirements for the degree of Diploma in Mechanical Engineering at the University of Thessaly

Volos, 2022

Approved by the Committee on Final Examination:

Advisor	**Dr. Spyros A. Karamanos**, Professor of Structural Mechanics, Department of Mechanical Engineering, University of Thessaly
Member	**Dr. Costas Papadimitriou**, Professor of Structural Dynamics, Department of Mechanical Engineering, University of Thessaly
Member	**Dr. Konstantinos Ritos**, Assistant Professor in Compressible Flows - Turbomachinery, Department of Mechanical Engineering, University of Thessaly

Date Approved: [, 2022]

Acknowledgements

STRUCTURAL ANALYSIS OF A STEEL FLOATING PLATFORM FOR THE SUPPORT OF A 10 MW WIND TURBINE

GEORGIOS PAPADOPOULOS

Department of Mechanical Engineering, University of Thessaly

Supervisor: Dr. Spyros A. Karamanos

Professor of Structural Mechanics, Department of Mechanical Engineering, University of Thessaly

Abstract

Over the last years, sustainable forms of energy are gaining more attention with the ultimate target to reduce the dependency of everyday life on conventional fuels for energy production. Offshore wind is a relentless source of sustainable power, and the progression of technology could broaden the potential of offshore wind industry. Floating wind turbines are a relatively new concept that has the potential to dominate the offshore wind industry. REFOS has been an innovative project (2016-2019) aiming at developing a multi-purpose steel floating platform suitable for the combined exploitation of wind and wave energy. This platform will host a 10 MW offshore wind turbine and will be equipped with special arrangements that extract wave energy. Such hybrid systems have not constructed yet and REFOS floating project could offer a breakthrough to the existing offshore wind technology. The general purpose of REFOS structure is to achieve an optimum structural solution for the platform, by combining offshore, wind, and wave engineering concepts with a structural engineering practice.

In this thesis, the optimization of an existing numerical structural model of the REFOS platform was performed. That model was developed using a general-purpose finite element program (ABAQUS) and simulates the global response of the platform against a combination of hydrostatic and extreme hydrodynamic loads that originate from the environmental conditions of the installation location. The already developed numerical problem had major convergence issues and increased computational cost. A large-scale optimization procedure was followed mainly focusing to enhance the computational efficiency of the existing numerical model. For that reason, major improvements to the quality of mesh and the modelling of interactions between the parts of the structure were performed. With continuous troubleshooting, a functional numerical model which predicts the global response of the structure was finally obtained. The global response of the system calculated in this thesis, provides a depiction of the stress and displacement of the components of the platform. The stresses were computed aiming at locating the critical regions of the structure, i.e., the parts of the platform that the highest stress concentrations occur, making them possible

locations for initiation of failure. The target of the analysis is to examine the local failure mechanisms that could occur in the critical regions, so that to obtain a future estimation of the design life of the structure. In case that the desired structural strength of the platform is not achieved, new design concepts would be tested more directly using the improved numerical model.

It was concluded that to study more effectively the local phenomena at the critical regions of the structure, a local scale model should be developed containing only the points of interest. The development of the local scale model will be based on the global response of the structure at those specific locations. The stress field at the vicinity of critical regions will be extracted and used as boundary conditions for the local scale numerical model. Thus, this stress field should be smooth and reliable for the effective transition from the global to the local scale. Thus, besides improving computational efficiency of the global model, in this thesis several attempts to enhance the stress distribution around critical regions were performed.

Future designs are proposed aiming at relieving the critical regions of the structure from the high stress fields. Apart from the structural point of view, a reduced fabrication cost of the platform is desirable to make more viable its production. Improvements on the initial geometry of the structure focus on the weight reduction of the platform, while ensuring the required structural stability.

ΔΟΜΙΚΗ ΑΝΑΛΥΣΗ ΧΑΛΥΒΔΙΝΗΣ ΠΛΩΤΗΣ ΠΛΑΤΦΟΡΜΑΣ ΓΙΑ ΤΗ ΣΤΗΡΙΞΗ ΑΝΕΜΟΓΕΝΝΗΤΡΙΑΣ ΙΣΧΥΟΣ 10 MW

ΓΕΩΡΓΙΟΣ ΠΑΠΑΔΟΠΟΥΛΟΣ

Τμήμα Μηχανολόγων Μηχανικών, Πανεπιστήμιο Θεσσαλίας, 2022

Επιβλέπων καθηγητής: Δρ. Σπύρος Καραμάνος

Καθηγητής Μηχανικής των Κατασκευών

Περίληψη

Στην πάροδο των τελευταίων χρόνων οι βιώσιμες μορφές ενέργειας κερδίζουν όλο και περισσότερη προσοχή με απώτερο σκοπό τη μείωση της εξάρτησης της καθημερινής ζωής από τα συμβατικά καύσιμα για την παραγωγή ηλεκτρικής ενέργειας. Ο υπεράκτιος άνεμος είναι μια ατελείωτη μορφή ανανεώσιμης ενέργειας και η εξέλιξη της υπάρχουσας τεχνολογίας θα μπορούσε να διευρύνει την δυναμική της υπεράκτιας αιολικής βιομηχανίας. Οι πλωτές ανεμογεννήτριες έχουν την προοπτική να κυριαρχήσουν στην αιολική βιομηχανία, όμως η ευρεία εφαρμογή τους βρίσκεται ακόμη σε ερευνητικό στάδιο. Το REFOS (2016-2019) υπήρξε ένα καινοτόμο ερευνητικό σχέδιο με σκοπό την ανάπτυξη μιας χαλύβδινης πλωτής πλατφόρμας, ιδανική για την ταυτόχρονη εκμετάλλευση αιολικής και κυματικής ενέργειας. Η πλατφόρμα θα χρησιμοποιηθεί για την στήριξη μιας πλωτής ανεμογεννήτριας ισχύος 10 MW, ενώ θα φέρει ειδικές διατάξεις για ταυτόχρονη εκμετάλλευση κυματικής ενέργειας. Τέτοιου είδους πλωτά συστήματα δεν έχουν κατασκευαστεί ακόμη και έτσι το ερευνητικό σχέδιο REFOS έχει την προοπτική να προσφέρει σημαντική πρόοδο στην υπάρχουσα τεχνολογία. Ο σκοπός της πλατφόρμας του REFOS είναι η επίτευξη του βέλτιστου δομικού σχεδιασμού της κατασκευής ώστε να ανταποκριθεί επαρκώς στις απαιτητικές περιβαλλοντικές συνθήκες.

Το κύριο αντικείμενο της παρούσας διπλωματικής είναι η βελτίωση ενός ήδη υπάρχοντος αριθμητικού μοντέλου πεπερασμένων στοιχείων , που προσομοιώνει την απόκριση της πλατφόρμας του REFOS σε ένα συνδυασμό υδροστατικών και μέγιστων υδροδυναμικών φορτίων. Το μοντέλο αυτό είχε δημιουργηθεί με το πρόγραμμα ABAQUS και εμφάνιζε σημαντικά προβλήματα σύγκλισης σε συνδυασμό με ένα πολύ μεγάλο υπολογιστικό κόστος. Ακολουθώντας μια εκτεταμένη διαδικασία βελτιστοποίησης του ήδη υπάρχοντος αριθμητικού μοντέλου, επιτεύχθηκε η σύγκλιση του υπολογιστικού αλγόριθμου, ενώ το υπολογιστικό κόστος μειώθηκε σημαντικά. Για το σκοπό αυτό, έγιναν σημαντικές αλλαγές στην ποιότητα του πλέγματος των πεπερασμένων στοιχείων, καθώς και στον τρόπο αλληλεπίδρασης των δομικών στοιχείων της πλατφόρμας. Με συνεχείς διορθώσεις, το ήδη υπάρχον μοντέλο έγινε λειτουργικό και η απόκριση του συστήματος υπολογίσθηκε. Η ολική απόκριση που υπολογίσθηκε στα πλαίσια της παρούσας διπλωματικής, περιλαμβάνει την αποτύπωση του πεδίου τάσεων και παραμορφώσεων στα δομικά στοιχεία της κατασκευής. Οι τάσεις υπολογίσθηκαν με σκοπό των εντοπισμό των κρίσιμων σημείων της κατασκευής,

των σημείων δηλαδή όπου υφίστανται υψηλές συγκεντρώσεις τάσεων κάνοντας τα πιθανές τοποθεσίες για αρχή δομικής αστοχίας. Ο στόχος της ανάλυσης είναι να εξετασθούν οι τοπικοί μηχανισμοί αστοχίας στις κρίσιμες περιοχές της κατασκευής, και έτσι να γίνει μια μελλοντική εκτίμηση του κύκλου ζωής της πλατφόρμας. Σε περίπτωση που η αντοχή της κατασκευής δεν είναι η επιθυμητή, αλλαγές στο σχεδιασμό της κατασκευής μπορούν να εξεταστούν χρησιμοποιώντας το βελτιωμένο αριθμητικό μοντέλο.

Για να μελετηθούν πιο αποδοτικά τα τοπικά φαινόμενα στις κρίσιμες περιοχές της κατασκευής, ένα τοπικό αριθμητικό μοντέλο πρέπει να δημιουργηθεί που θα περιλαμβάνει μόνο τα κρίσιμα σημεία. Η κατασκευή του τοπικού μοντέλου θα βασιστεί στα αποτελέσματα της προσομοίωσης του της ολικής κατασκευής. Οι τάσεις γύρω από τα κρίσιμα σημεία θα απομονωθούν και θα χρησιμοποιηθούν ως συνοριακές συνθήκες στο τοπικό μοντέλο. Έτσι, η κατανομή των τάσεων γύρω από τα κρίσιμα σημεία θα πρέπει να είναι όσο το δυνατόν πιο ομαλή και αξιόπιστη ώστε να γίνει η μετάβαση από το ολικό στο τοπικό μοντέλο. Οπότε ένας ακόμη στόχος της παρούσας διπλωματικής είναι η βελτίωση της κατανομής των τάσεων γύρω από τις κρίσιμες περιοχές.

Μελλοντικές ιδέες προτείνονται με σκοπό να αποσυμφορηθούν οι κρίσιμες περιοχές από τις υψηλές συγκεντρώσεις τάσεων. Εκτός από την οπτική του δομικού σχεδιασμού της πλατφόρμας, η μείωση του κατασκευαστικού κόστους της διάταξης θα κάνει πιο βιώσιμη την κατασκευή της. Έτσι παρατίθενται ιδέες για βελτίωση της αρχικής γεωμετρίας ώστε να μειωθεί το βάρος της κατασκευής, ενώ παράλληλα να διατηρηθεί η δομική ευστάθεια.

Contents

List of figures

List of tables

1 Introduction

Currently, there is an international tendency to reduce the dependency on conventional fuels for electricity production and turn into sustainable forms of energy. To achieve that, the amount of renewable energy share at the total energy production must be amplified. At this point, wind is the second most widely used renewable energy source globally, behind hydropower, but as it will be explained later it has boundless potential. Wind energy exploitation is becoming more and more popular. Offshore wind energy is getting constantly increasing attention, as it has much more energy potential from the onshore wind industry. In the sea, stronger and more regular winds exist and that allows to use bigger wind turbines. There are also significantly fewer spatial restrictions compared to the land. Additionally, there is less visual impact especially if the wind turbines are located far from the sore. Thus, developing more offshore wind farms appears to be an ideal solution, to further increase the sustainability of electrical energy. The majority of the current offshore wind farms is comprised of wind turbines with bottom-fixed foundations. The technology of bottom-fixed foundations is relatively mature and has been successfully deployed to the development of large-scale offshore wind farms. Many countries do not have shallow coastal shelf, and therefore the development of such offshore wind farms won't be cost-effective since their cost is strongly affected by the sea depth. Floating wind turbines could be the ideal solution for that problem, since they are the most cost-competent configuration for water depths larger than 80m. [Figure 1] There are no commercial farms of floating wind turbines yet, but many proposed designs are investigated and several prototypes are being tested on the sea. Despite being a promising project the floating wind turbines appear to undergo much greater fatigue and environmental loading compared to the bottom-fixed wind turbines. Thus, those structures need to be more robust, and hence more expensive than the fixed ones. An effective design of a floating structure that will have the required structural stability and the least possible fabrication cost will be a step forward to the existing technology and will broaden the potential of wind energy. A major extension to the floating wind turbines project is their combination with integrated wave energy converters, so that wind and wave absorption occurs at the same time. This is a new concept which will offer a breakthrough at the existing offshore wind technology. [7]

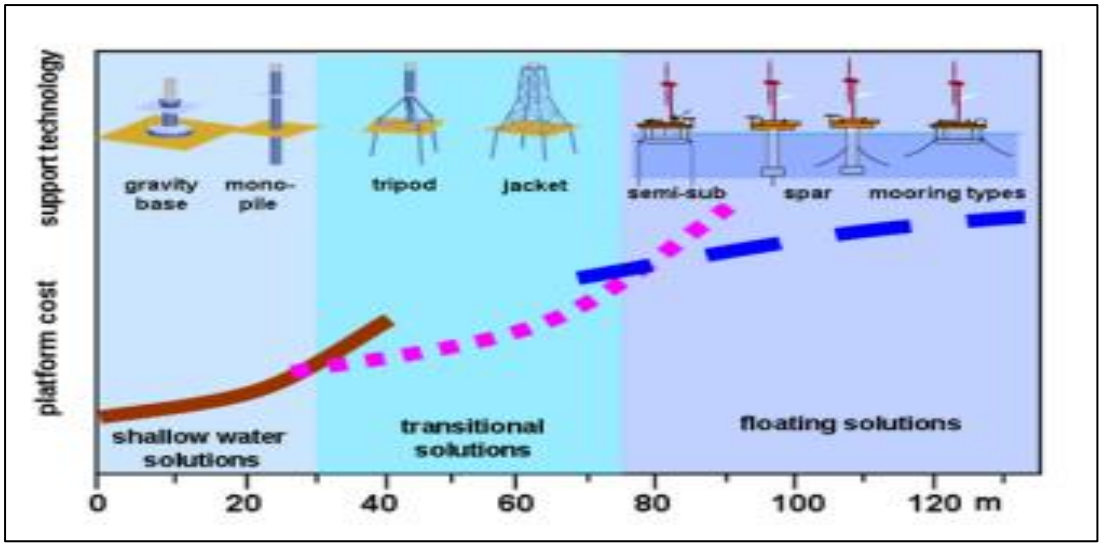

Figure 1. Cost of different designs of platforms as a function of sea depth.

REFOS (2016-2019) has been an innovative project aimed at developing a multi-purpose steel floating platform that will be used for the combined exploitation of wind and wave energy. The major target of the project was the development of a complete design of the platform and its components, providing final design report as well as specific drawings for three ideal installation locations. Those areas have been selected because they meet the appropriate climate criteria, meaning that they provide the required wind and wave potential, and they are at 200m depth. Two of them are located at the Mediterranean Sea and the other at the North Sea. Wave energy is extracted by wave converters which are attached to the platform. The integrated wave converters would increase 6-8% the power output of the Wind Turbine (WT), and thus covering the maintenance costs of the whole structure, which is estimated to be 2% of the wind power output. One of the main sectors that this project consists of is the structural design of the steel floating platform that will carry the 10 MW WT. The general purpose of REFOS structure is to achieve an optimum structural solution for the platform, by combining offshore, wind, and wave engineering concepts with a structural engineering practice. [7] Another part of the optimum design is to maintain maximum energy output while limiting to the minimum the installation, construction, and operational costs. Such systems with combined exploitation of wind and wave energy have not been constructed yet and REFOS would offer a breakthrough in renewable energy industry. [7]

REFOS project would contribute to the further progression of the existing technology, aiming at making more viable the future development of such hybrid configurations and therefore set the basis for their future large-scale implementation. Since wind is a relentless source of power, hybrid floating wind turbine concepts open a new horizon to sustainable energy source and lead to the further evolution of the offshore wind industry. With the commercial development of such configurations, the

amount of potential renewable energy could escalate leading to a more sustainable future.

Preliminary design calculations have already been performed resulting to a complete geometry of the platform and its components which will be depicted in chapter 2. To ensure the safety of the REFOS floating platform, the following design requirements must be considered. Firstly, the platform should be able to support the 10 MW offshore WT, while providing the sufficient rigidity to the WT, to sustain the dynamic loads during its operation. Furthermore, it must operate for a design life of at least 20 years and withstand the extreme loading conditions that could occur during the structure lifetime. A detailed numerical model has been developed for that reason using a general-purpose finite element software (ABAQUS). That model includes the exact geometry of the floating structure and simulates the interaction of the platform with a combination of hydrostatic and hydrodynamic loads. Those loads originate from the surrounding environment of each installation site and consist of ocean waves, sea currents and wind gusts.

The already developed numerical model though, had major convergence issues and increased computational cost. In this thesis, the enhancement of that initial numerical model will be performed, aiming at developing an improved numerical model that will predict efficiently the global response of the structure and thus determine if the current design considerations are met.

1.1 Purpose of thesis

The development of a functional numerical model that predicts the global response of the platform with low computational cost, is the key tool for the improvement of platform's structural design. It is necessary to obtain a reliable estimation of the design life of the structure. Furthermore, the simulations could be used to determine if the current geometry of the structure is suitable for meeting the sustainability targets of the project, and in case that it isn't, new design ideas could be tested. A flexible and reliable numerical model is the tool to try small-scaled geometry alterations on the initial design to find the optimum configuration that will yield to the required structural strength of the platform, with the use of the least possible material. That will benefit the economic sustainability of the project, since the fabrication cost of the platform, which is proportional to its weight, will be reduced. As it will be defined in the next chapter the platform has large-scale dimensions and complex geometry. The development of a functional numerical model becomes crucial especially for such complex geometries, since it's the only straightforward way to simulate the response of the structure to a variety of loading cases.

The reason for conducting research on this specific floating wind turbine design concept is that REFOS project could set a breakthrough to the existing technology leading the way to a more sustainable energy production. The innovative

configuration that allows the combined extraction of wind and wave energy increases the energy output of the wind turbine. Structural enhancement of the platform is necessary to bring that design proposal to realistic implementation, since it must secure that the platform is sustainable from the structural and economical point of view. First, the platform should be designed to sufficiently sustain the induced loads during its lifetime period, which should be at least 20 years. Subsequently, the design must ensure total investment payback and satisfactory profit from the energy output of the system.

1.2 Contribution of the present thesis.

The ultimate target of this thesis is the development of an improved numerical model that will predict the global response of the structure with a relatively narrow time limit. An extensive effort was made on modifying and enhancing the initial numerical model, mainly focusing on the improvement of its computational efficiency. Starting from that initial model which required continuous troubleshooting of solution process, a functional numerical model was finally obtained. The optimization process that was followed, had the following sequence of actions. Initially, major changes in finite element mesh quality and density were performed resulting in an enhanced finite element mesh in all surfaces of the model. Subsequently, the interactions between the parts of the numerical model were examined, and critical improvements were made in contact algorithms that contribute to overcome the convergence problems. The results were that desired numerical convergence ratios were achieved, and the simulation time was significantly reduced. In spite the fact that a functional model with increased numerical convergence is vital, reliability of the obtained results, especially at the points of interest is a crucial parameter. Thus, different ways were investigated to obtain a smoother stress distribution, mainly by increasing the mesh density at the critical points of the structure, while ensuring that there is no mesh distortion. Critical points are the regions of the model that high stress concentration factors occur, making them possible locations for initiation of failure. Those regions are quite important for the design life of the structure since they intensely affect the structural strength of the platform. By examining the results from the global analysis, critical regions of the structure were located.

The specific analysis is a multiscale structural mechanics problem, since the platform is a large-scale structure, and the failure would occur only at some specific regions. The obtained global response of the structure could not provide satisfactory results at the local scale of the critical regions. A future step is to develop a local model to examine more effectively the possible failure mechanisms at the vicinity of critical regions and therefore obtaining a reliable estimation of structure's design life, which must be at least 20 years. As it will be analyzed further in the next chapters, the global response of the structure and especially the stress field around critical regions is essential to make the transition from the global to the local scale. That's why a target of the current thesis is to ensure smooth stress distribution at those regions. If the current design considered to be inappropriate to achieve the sustainability targets of the whole project, redesign is necessary to obtain the desired behavior.

1.3 Outline of thesis

A brief outline of the following chapters is provided below.

- In chapter 2, the geometry of the platform and its components is described aiming to familiarize the reader with the general design of the system
- In chapter 3, the improved numerical model that depicts the platform's geometry is presented and the optimization procedure that was followed is pointed out.
- In chapter 4, the results of the simulation are outlined, mainly focusing on the stress distribution around specific parts of the system and around the critical regions of the structure.
- In chapter 5, overall conclusions about the total procedure that was followed in that thesis and the sustainability of the whole project are provided.
- In final chapter, which is the chapter 6, the future steps that could optimize even further the analysis are represented.

2 Description of supporting steel structure

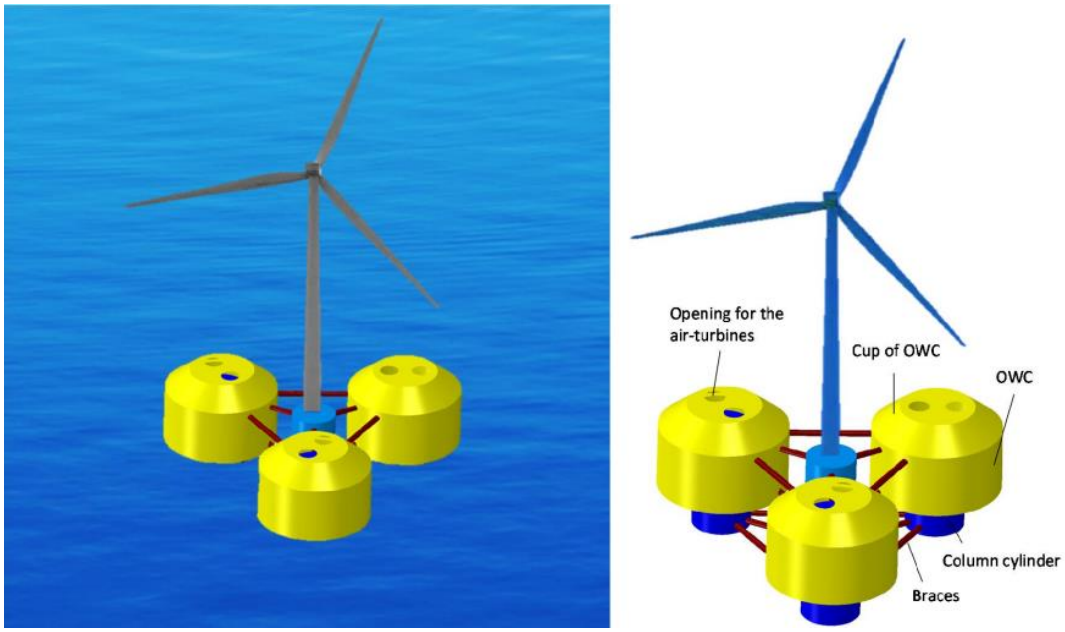

Figure 2. Schematic representation of REFOS platform [12]

The REFOS platform consists of a triangular arrangement of cylindrical pontoons that are interconnected with steel braces. Different views of the structure are depicted at Figure 2 and Figure 3. Three circumferential cylinders called also offset columns, are placed symmetrically around a central cylinder (configurations with blue color on Figure 2, Figure 3). Steel tubular braces are used to join the offset columns with each other as well as with the central cylinder. A water column device (OWC), being the configuration with yellow color on Figure 2 and Figure 3, is attached on each of the circumferential column cylinders. The central cylinder is the one that the tower of the 10 MW wind turbine will be cantilevered on, at an elevation of 10 meters above the sea water level (SWL). The platform is anchored to the seabed, at a depth of 200m below the SWL, using a TLP mooring line system. The depth of the platform below SWL is 20m.[8] A complete representation of the system is depicted at Figure 3 to help the reader conceive the large-scale dimensions of the structure. In the next paragraphs, each of the main components of the platform will be analyzed so that the reader will be familiarized with the general design.

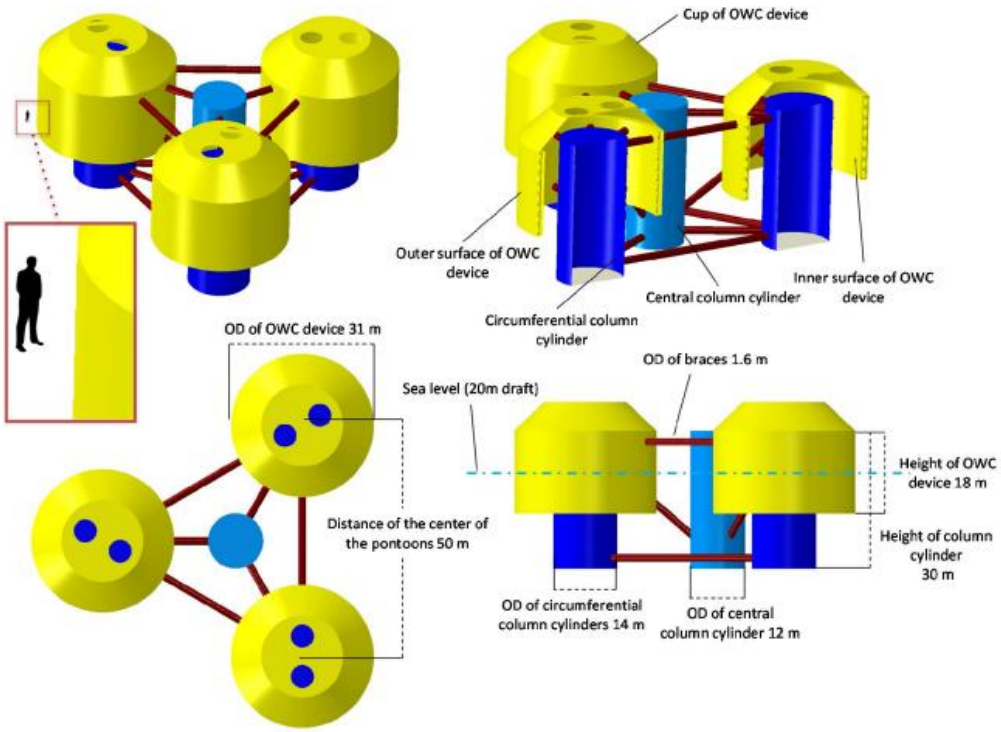

Figure 3. General dimensions of the total structure [12]

The main parts of the platform are the arrangement of column cylinders with their stiffeners, the system of braces, the mooring line system and the OWC devices that include the OWC chambers, the conical casing, and the truss structure.

2.1 OWC devices

OWC is a type of wave energy converters. They consist of a semisubmersible cylindrical body that covers the existing circumferential cylinders, resulting in an annular chamber. That hollow chamber is open from its bottom end, allowing sea water entering through it. The upper end is insulated by a conical cup. So, this configuration is filled with water till SWL, while the rest part is filled with air (Figure 4). The vertical motion of the sea surface acts like a piston, as it continuously compresses and decompresses the air trapped inside the chamber, resulting in a reciprocating flow of air. That flow comes through an air turbine that is installed beneath the roof of OWC device and is coupled with an electric generator.

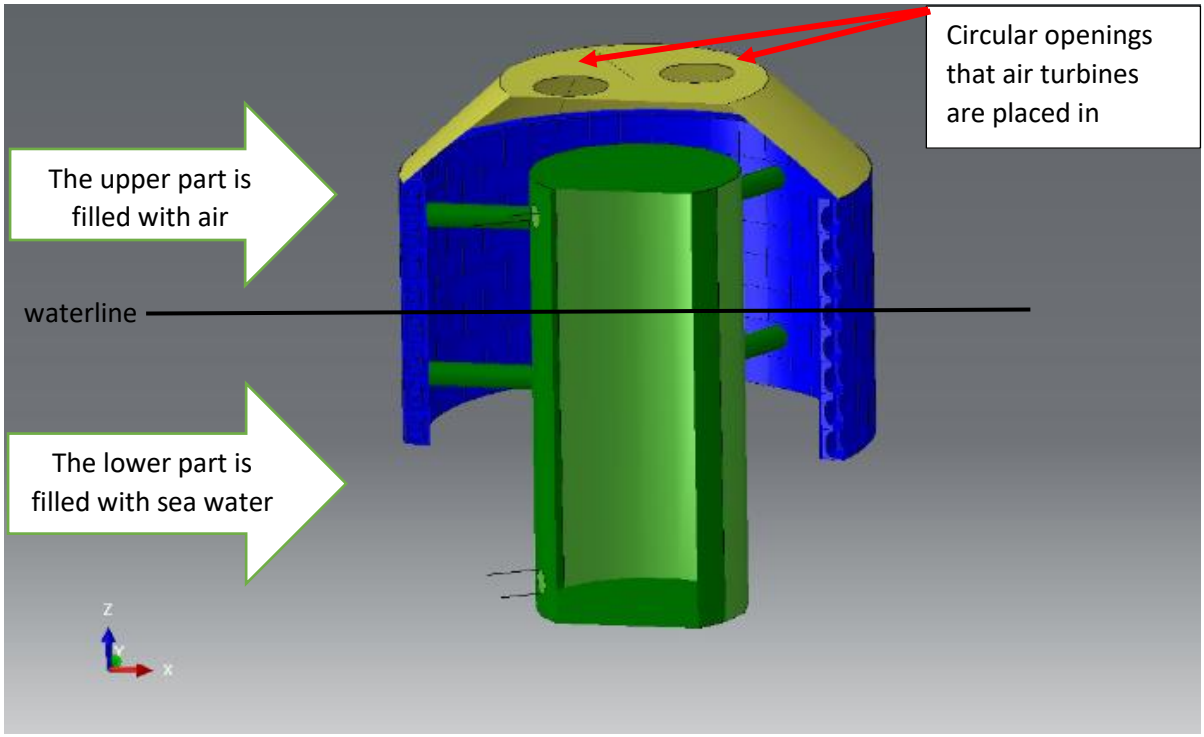

Figure 4. Inside view of a OWC chamber. The truss structure that holds the conical casing is not visible.

The vertical distance between the waterline and the bottom of each part is called draught or draft. Thus, the draught is the length of the submerged region of a structure. The draught, thickness, and the diameter of the OWC chambers have been determined to maximize the generating power. Calculations have been conducted using different values for the above parameters and the optimum dimensions were determined. Konispoliatis et al. (2016) showed that the thickness and draught of the chambers are inversely proportional to the power output, while the diameter is proportional to the power output. The dimensions that optimize the power output of OWC device were calculated and they are 14 m for the internal diameter, 1.5 m for thickness of OWC chamber and 8m for draught [5].

Table 1. Optimum dimensions of OWC chambers

Internal diameter	14m
Draught	8m
OWC chamber's thickness	1.5m

The complete configuration of the OWC device contains the cylindrical body, the conical cup and a truss structure that is used to support the conical casing.

2.1.1 Main body of OWC devices (OWC chamber)

The cylindrical body of the OWC is made of shell-type inner and outer surfaces, depicted at Figure 8, that are joined with a special system of stiffeners. That system is comprised of ring horizontal stiffeners (also called bulkheads) which are illustrated at Figure 6, and vertical stiffeners with elliptical openings that are depicted at Figure 5.

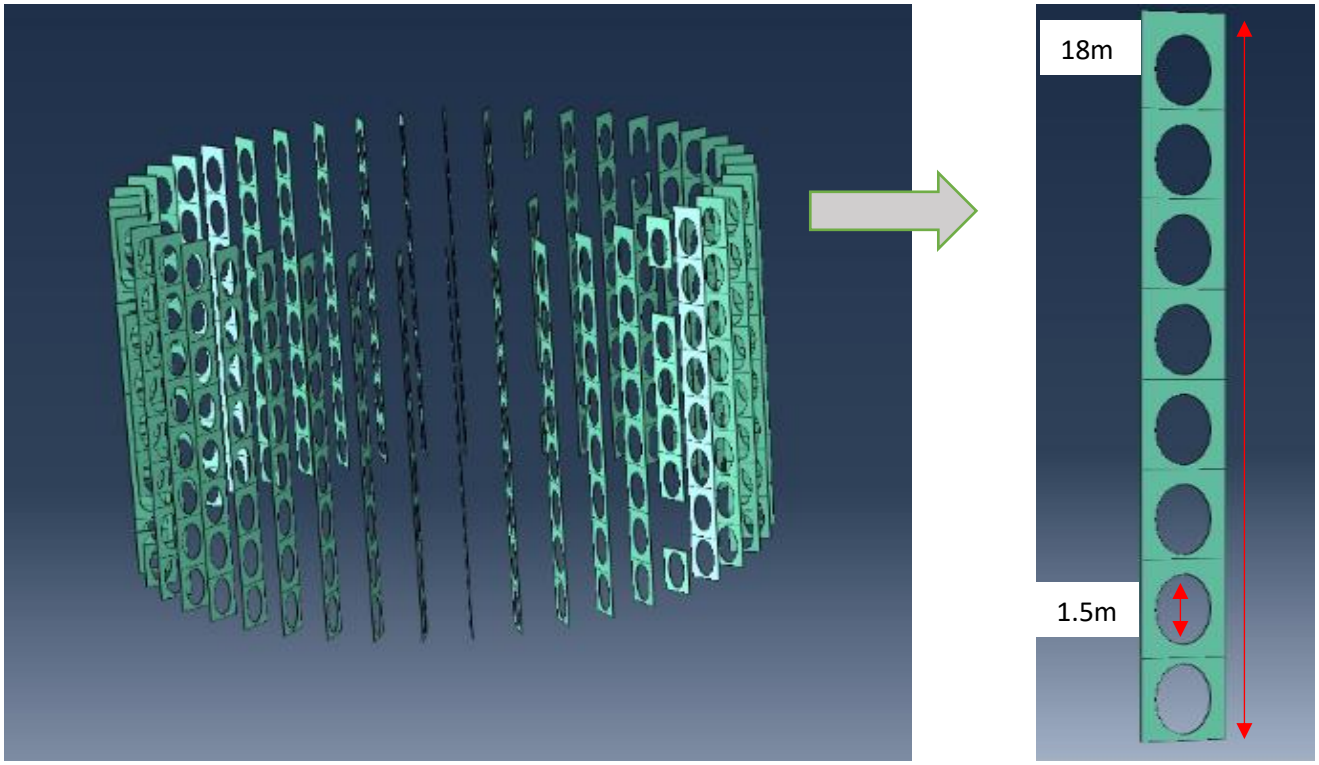

Figure 5. Vertical stiffeners of OWC devices.

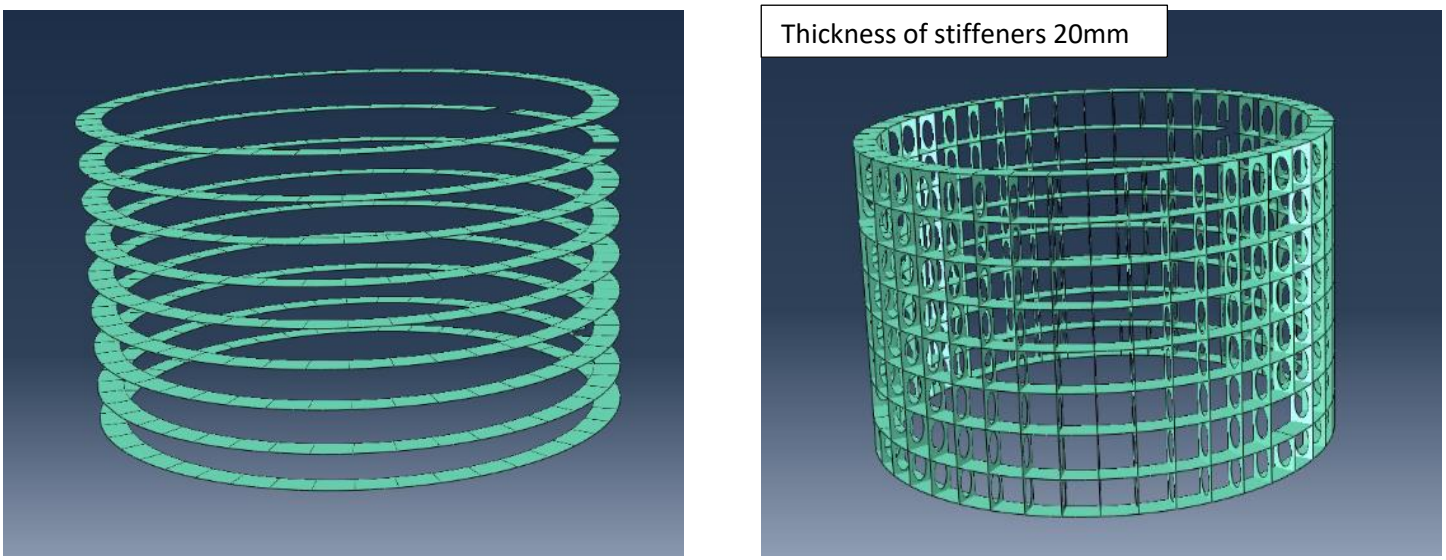

Figure 6. Left side: Horizontal OWC stiffeners. Right side: Horizontal and vertical stiffeners combined

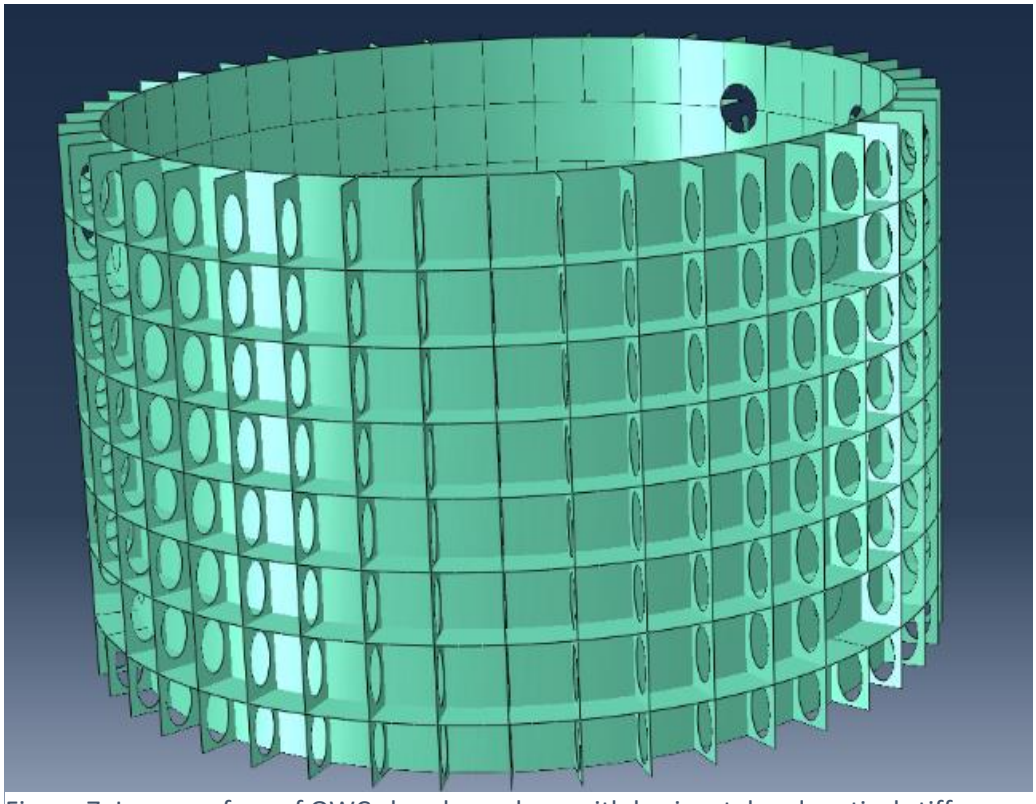

Figure 7. Inner surface of OWC chambers along with horizontal and vertical stiffeners

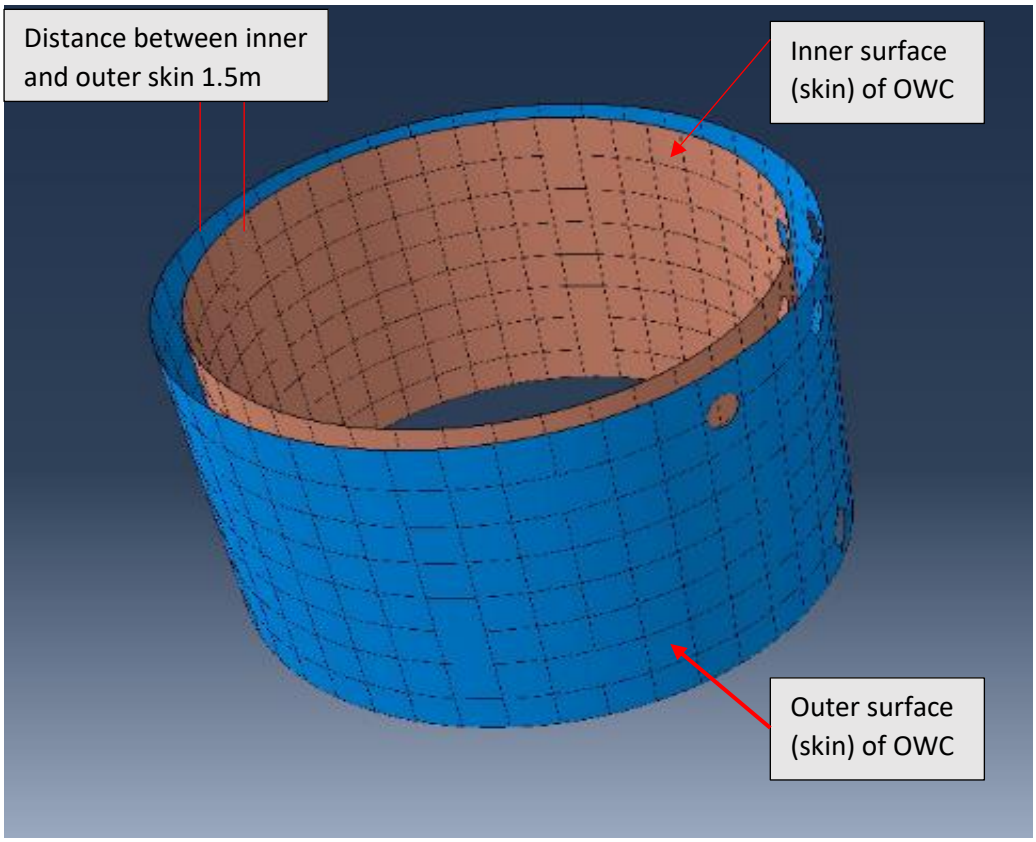

Figure 8. Inner and outer surfaces (skins) of the OWC chamber

As Figure 8 illustrates the distance between the inner and the outer surface of the chamber is 1.5m. The internal diameter of the OWC chamber is 28m and thus, the outer diameter is 31m. The cylindrical body of each OWC device is connected to the corresponding circumferential cylinder with a set of 6 steel braces. [See Figure 14]. The overall dimensions of the OWC chambers are described collectively at the Table 2.

Table 2. Dimensions of OWC chambers

Thickness of inner and outer skins	25mm
Thickness of stiffeners	20mm
Distance between inner and outer skin (or thickness of OWC chamber)	1.5m

Diameter of elliptical openings of vertical stiffeners	1.5m
Internal diameter of OWC chamber	28m
External diameter of OWC chamber	31m
Draught of OWC chamber	8m
Length of OWC chamber (draft + elevation above SWL=8+10=18m)	18m

2.1.2 Conical casing of OWC devices:

This part covers and seals each OWC device from the top, while the air turbines are placed at the circular openings of its top surface. A design requirement of conical casing is to be thick enough to endure the variable air pressure from the operation of OWC device. Thus, it's thickness was calculated to 5 mm [9]. The diameter of each of the circular openings is 5 m.

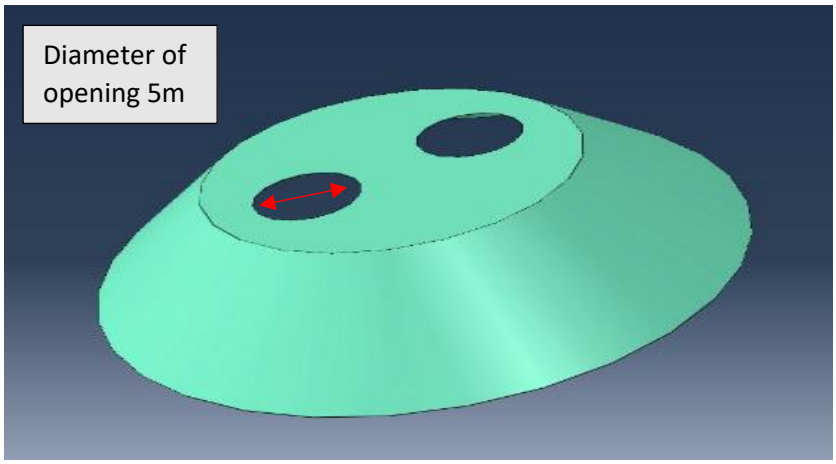

Figure 9. Conical casing of OWC device

2.1.3 Truss structure

To support the conical casing but also to reduce its weight, a truss structure has been placed between the conical cup and the upper surface of OWC chambers. [Figure 10]. It is made up of steel tubular beams with 0.15m diameter, while their thickness is 0.005m. The truss structure transfers safely the weight of the cup to the cylindrical body of the OWC device.

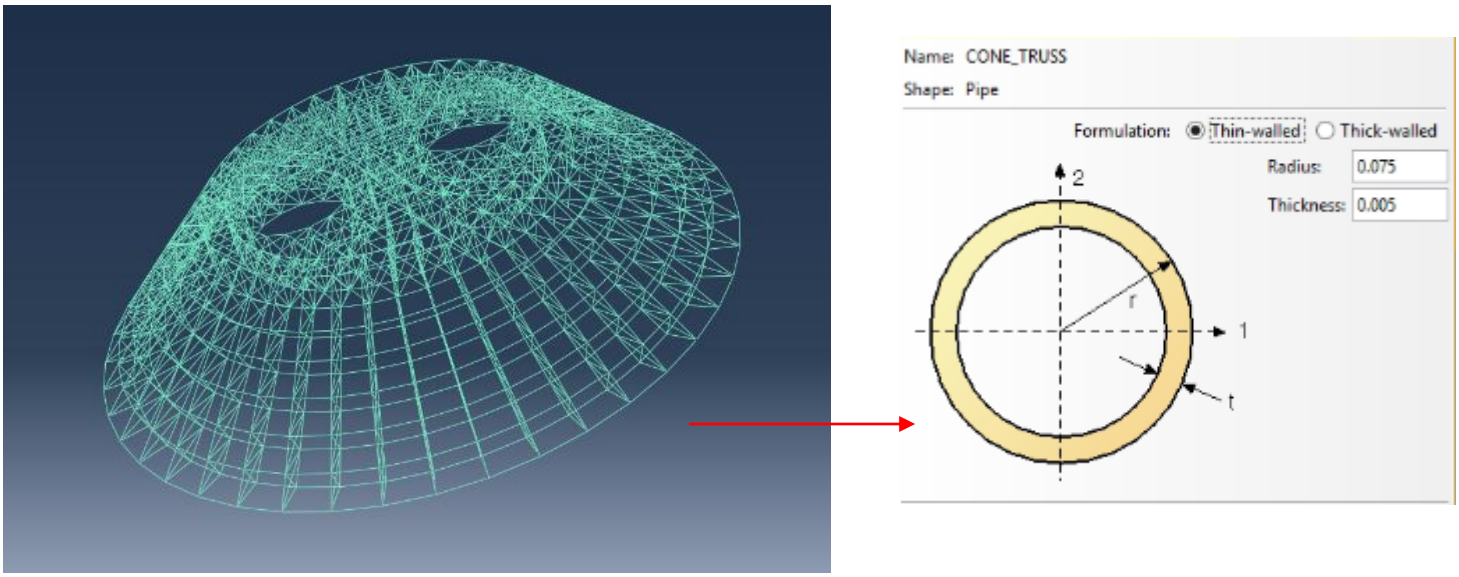

Figure 10. Truss that supports the conical casing made of steel tubular members

2.2 Column Cylinders:

Column cylinders are a configuration of hollow cylinders with a very high diameter over thickness ratio. They act as pontoons because their big volume and their relatively low mass help the structure to displace more water and therefore increase its buoyancy force. The 3 circumferential cylinders have a diameter of 14 m while the central one has a diameter of 12 m. Circumferential cylinders are separated in two equivalent surfaces with different thickness. The side that is closer to the central cylinder is thicker than the other one at a value of 35 mm, while the rest part has a thickness of 25 mm. That variation of thickness is justified as the loads from the rest of the platform are transferred to the thicker side through the braces that interconnect each circumferential cylinder to the other ones. The central cylinder has a constant thickness of 35 mm. Figure 11 depicts the arrangement of column cylinders. The variable thickness is illustrated with the difference in color. The elevation of column cylinders is 10 m above SWL. Central cylinder is the one that the tower of the WT will be attached. Since the draft of the platform is 20 m below SWL, the total length of each cylinder is 30 m. The basic dimensions of column cylinders are summarized at Table 3.

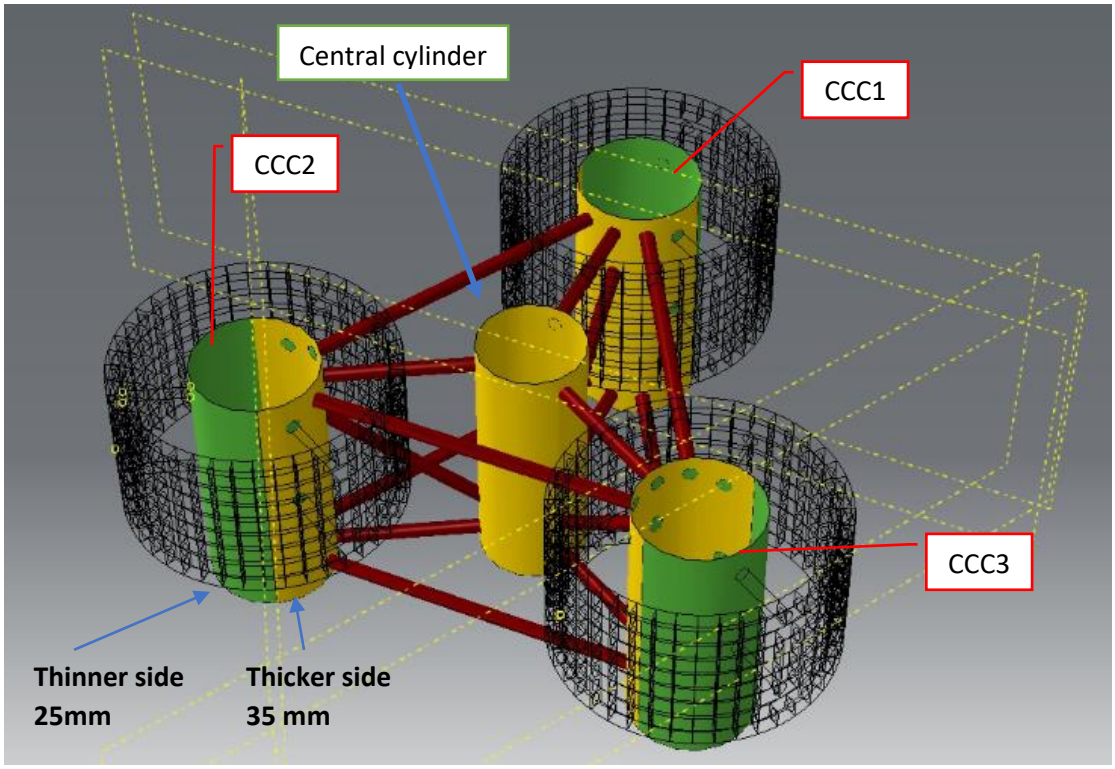

Figure 11: Arrangement of column cylinders. CCC → Circumferential Column Cylinder

Those cylindrical columns are reinforced with longitudinal and ring stiffeners of T profile which are illustrated at Figure 13. 15 ring type stiffeners and 34 longitudinal have been used in the circumferential column cylinders, arranged with spacing of 2.16 m and 1.30 m respectively. For the central cylinder, 20 ring and 35 longitudinal stiffeners were attached, positioned with 1.57 m and 1.30 m spacing respectively. [13] The cross-section dimensions of the stiffeners are depicted in Figure 12.

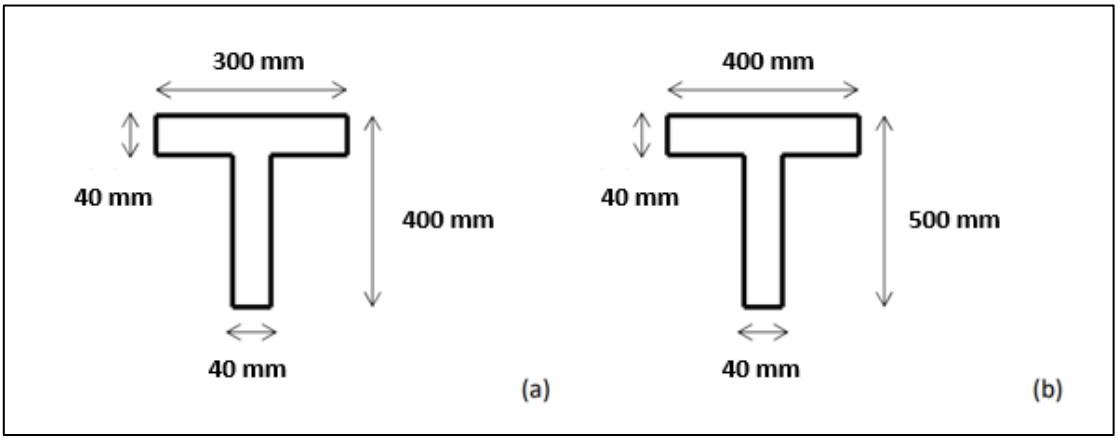

Figure 12.Cross section dimensions of ring stiffeners (a) and longitudinal stiffeners (b) [12]

Table 3. Dimensions of column cylinders

	Inner diameter (m)	Skin thickness (mm)	Total length (m)	Draught (m)
Circumferential column cylinder	14	25-35	30	20
Central column cylinder	12	35	30	20

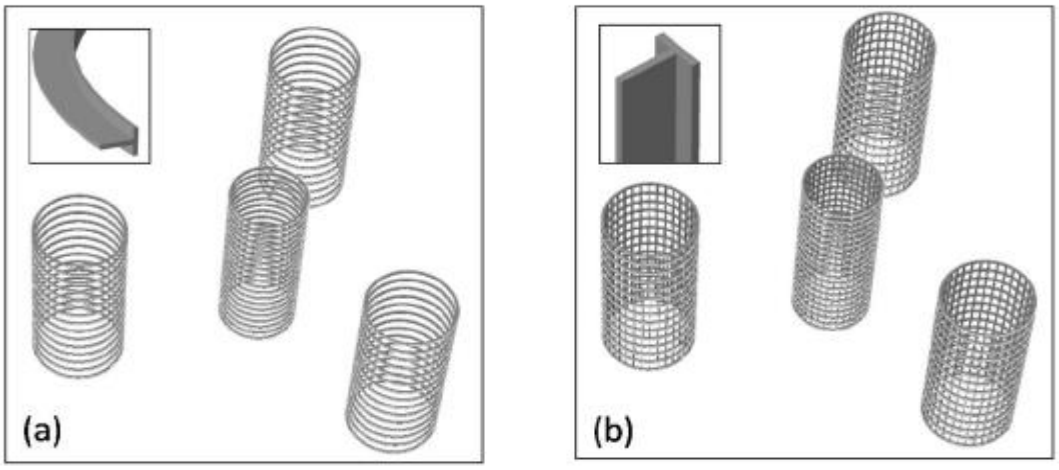

Figure 13: T-profile longitudinal and ring stiffeners assembled inside column cylinders [12]

2.3 Braces:

Tubular braces are used to join the different components of the platform. Another function of braces is that they act as pontoons since the submerged ones contribute to floatation of to the total structure by amplifying the buoyancy force, to exceed the structure's total gravity. Braces can be sorted in 3 main categories.

1) Braces that connect column cylinders with each other [Figure 15]
2) Braces that connect column cylinders with the central one [Figure 16 Figure 17]
3) Braces that connect OWC chambers with the circumferential column cylinders [Figure 14]

There are 2 sets of 3 horizontal braces which are used to connect the circumferential column cylinders with each other. Their length is 36 m. [Figure 15] Similarly, the same number of horizontal braces is used to connect the circumferential

cylinders with the central one, with length of 15.87 m [Figure 16]. There are also 3 additional cross braces for the connection of circumferential cylinders with the bottom part of the central. The length of each cross brace is 19.73 m [Figure 17] The three configurations are shown below. The last type of braces consists of 2 sets of 3 braces in each OWC device, resulting in 18 members in total with 7 m length each. [Figure 14] All braces have a thickness of 42.2 mm, while their outer diameter is 1.6 m.

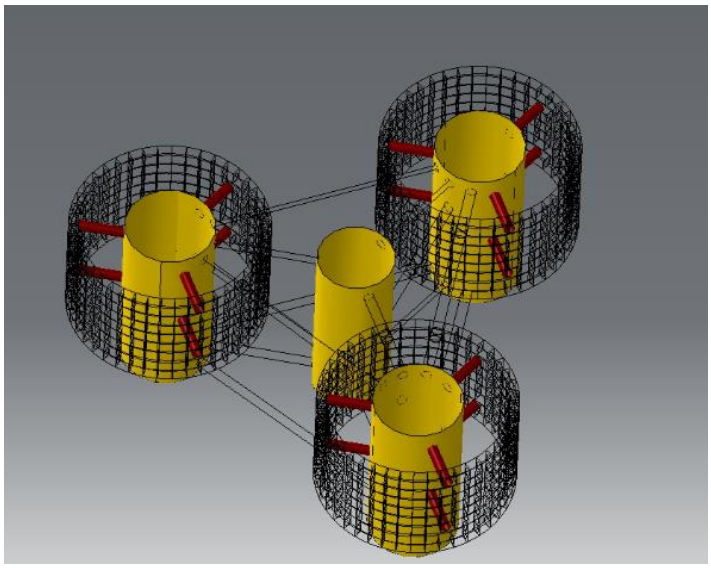

Figure 14. Braces that connect circumferential cylinders with OWC chambers. Length: 7 meters

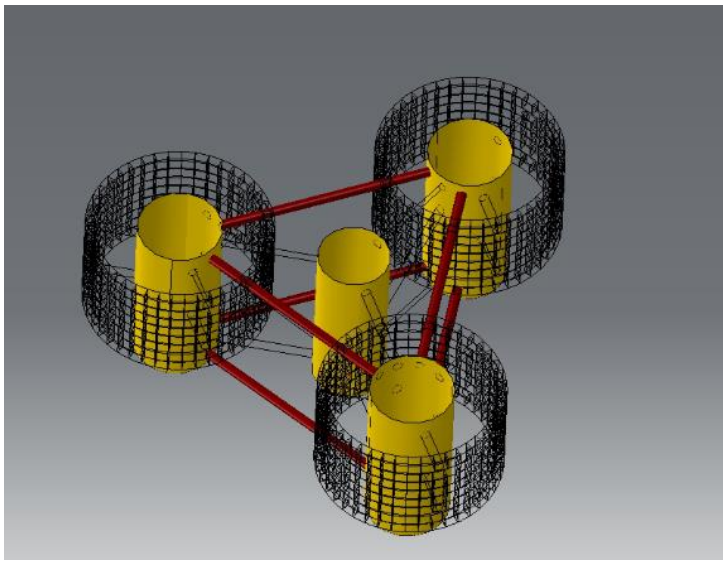

Figure 15. Braces that connect column cylinders with each other. Length: 36 meters

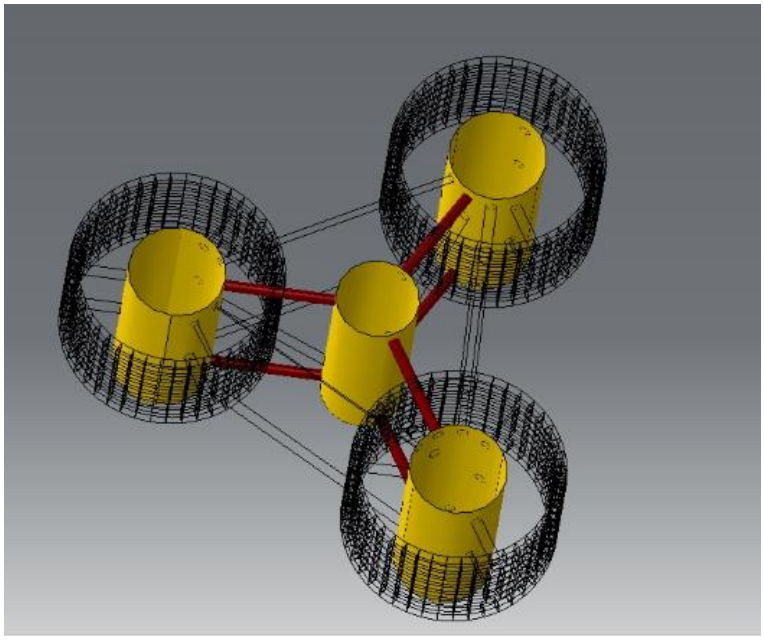

Figure 16. Horizontal braces that connect circumferential cylinders with the central one. Length of highlighted braces: 15.87 meters

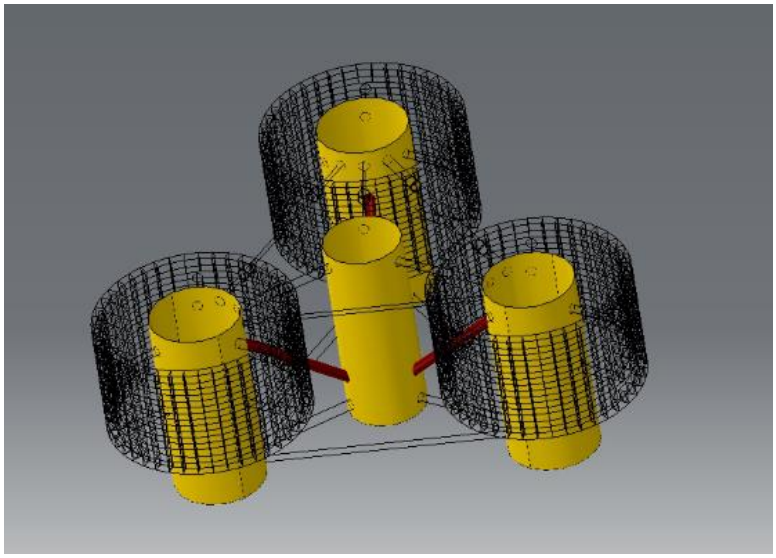

Figure 17. Cross braces. Length: 19.73 meters

2.4 Mooring line system:

There are several designs of platforms that are already implemented in the offshore oil and gas industry, that could be used to support floating wind turbines. They classified by the type of mooring line system used and the way that the platform is stabilized. Three representative designs are illustrated in Figure 19. Starting from the left configuration of Figure 19, the design of “Spar-buoy” support structure is depicted. A Spar type floating structure is a deeply submerged, vertical floating

structure, most commonly with a cylindrical shape, that supports the tower of the Wind Turbine and is moored to the seabed. [8] Semisubmersible support foundation consists of partially submerged vertical cylinders connected with braces. If we focus on the mooring line systems of Figure 19, we will realize that the above-described configurations have similar mooring line system. Spread mooring line systems with catenary lines are used to stabilize the Spar and Semisubmersible structures. Catenary line system is the most common mooring line system for shallow waters. Catenaries are used between the floating unit and the seabed, and they acquire that typical hanging line shape due to gravity. In the last supporting structure of Figure 19 the Tension Leg Platform (TLP) mooring line system is used, which is the configuration that has been selected to stabilize the REFOS platform. TLP refers to a platform that is secured by vertical tensioned pipes (tendons) which are connected to the floor using a foundation system. Foundation system includes templates that are kept in place by piles embedded to the seafloor. [8],[4]. TLP foundation is widely used to support offshore platforms for oil and gas production at water depths greater than 400 meters and less than 1500 meters. [Figure 18] TLP mooring system for hosting wind turbines, while having similarities with the equivalent used for oil industry, it differs in many aspects. A major variation is that conventionally moored platforms are allowed to perform controlled oscillations about a mean position, while TLP wind platforms must remain as much as possible still. [8]

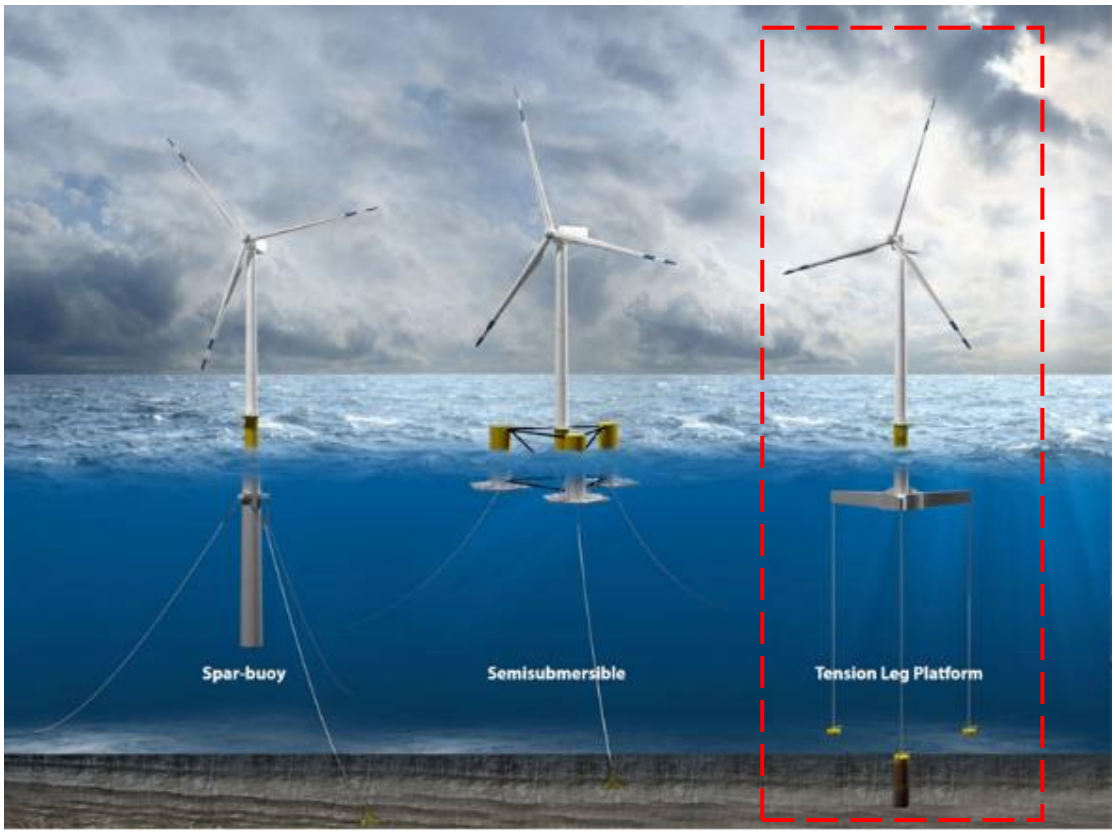

Figure 19. Typical designs of support structures for floating wind turbines. [6] Tension Leg Platform design concept has been employed in REFOS project.

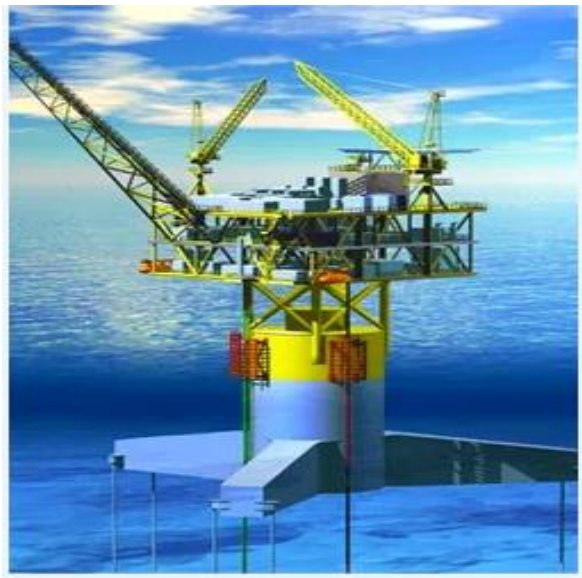

Figure 18. TLP platform used for offshore oil and gas industry.

The anchoring system of REFOS platform comprises six tendon pipes, two at each circumferential cylinder that are spread symmetrically along the vertical axis of the structure. As Figure 21 illustrates, the upper end of those tendons is attached at the bottom surface of the offset columns, at a 20m depth below the sea water level, while the lower end is located at the seabed at a water depth of 200m, resulting in a total tendon length of 180m. Rotating flexibility between both ends of tendon pipes is beneficial for the structure and for that reason a special connector arrangement that allows relative rotation of 10 degrees at maximum has been attached between tendon and hull of platform and between tendon and anchors in the seabed. After that value is reached, the connection locks disallowing any extra rotation. The tendons must be subjected to constant tension to limit the vertical platform motion (heave). A lateral motion of the tendons is allowed, and it is generated from the environmental loading of the platform (sea currents, waves, wind). The high tension of the tension legs though, limits horizontal offsets to a small percentage of the water depth. Tension legs of REFOS platforms have been designed to provide a maximum offset of 5% of water depth. [8] . Pretension of tendons is a crucial parameter, as it affects the axial displacement of the platform and thus it determines the stability of the structure during its operation. A high value of pretension results in stiffer tension legs and therefore limited axial movement of the platform. Additionally, sufficient pretension is required to level the large overturning moments, caused mainly by the operation of WT. [8]

Figure 20. Connectors attached to the top end (part on the left) and to the bottom end (part on the right) of tendons. [14]

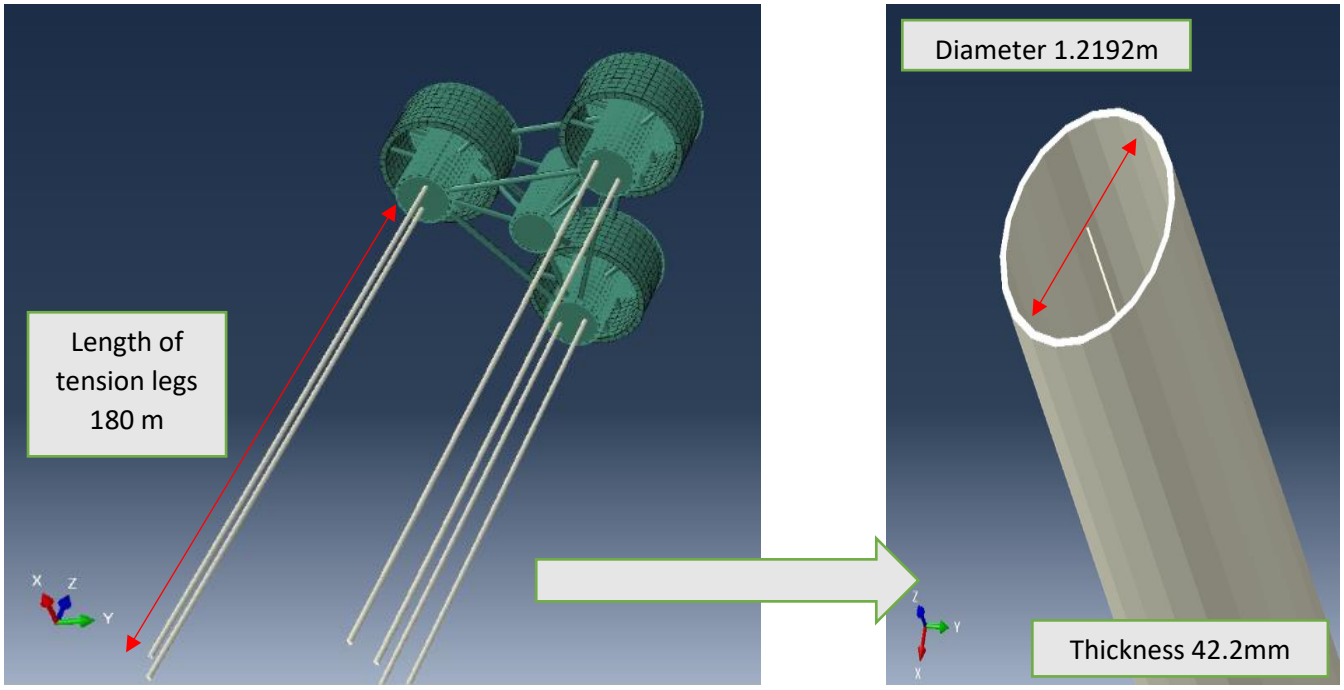

Figure 21. Attachment points of tension legs at REFOS platform (left) and basic dimensions of each mooring line (right).

In Table 4, an extensive description of the mass of the system is provided. The total mass of the platform and its components is stated, as well as the mass of the 10 MW Wind Turbine. Ballast is any additional material used to provide stability at the structure. The mass of ballast has been calculated to make the weight of the platform equal to its buoyant force, so that the system balances at the desired draught, which is 20 m below SWL.

Table 4. Mass of each component of the platform

Truss structure	89.43 tons
Conical casing	35.65 tons
OWC chambers with their stiffeners	967.59 tons
Central column cylinder with stiffeners	816.63 tons
Circumferential column cylinder with stiffeners	780.9 tons
Each tension leg on mooring line	220.48 tons
All mooring lines	1322.88 tons

Each brace of OWC	11.68 tons
All braces of the platform	834 tons
Ballast at central cylinder	401.85 tons
Ballast at each of circumferential cylinders	196.43 tons
Mass of 10 MW WT	1100 tons
TOTAL MASS OF PLATFORM (including ballast)	9553 tons
TOTAL MASS OF PLATFORM without ballast	8561 tons
TOTAL MASS OF SYSTEM including platform, ballast, and the 10 MW Wind Turbine	10653 tons

2.5 Materials of the parts of the platform

The materials used for the components of the platform are the X70 grade steel and S355 steel. X70 was used for the tendons, while S355 was used for the rest parts (OWC chambers, conical casing, truss structure, column cylinders and stiffeners).

- X70 is a premium grade piping material with minimum yield strength of 485 MPa. It has application on oil and gas transmissions. An elastic modulus of 200 GPa and a Poisson ratio of 0.3 was used for the analysis. The X70 material density is 7850 kg/ m^3
- S355 is a structural grade steel with a minimum yield strength of 355 MPa. It has low carbon percentage, approximately of 0.2% and it is used in demanding environments, such as the offshore industry. The elastic modulus of S355 is 210 GPa, the Poisson ratio is 0.3, and the material density that was used for the analysis is 7850 kg/m^3.

The general design of the floating structure meets the methodology described in DNV guidelines about offshore steel structures. (DNV-OS-C101, “Design of Offshore Steel Structures, General”) The shell components of the platform meaning the central and circumferential column cylinders, have been checked against elastic buckling of stiffened shells. In both parts, the design equivalent Von Mises stress was less than their shell buckling strength, which is the stability requirement for stiffened shells against axial compression and bending. Thus, the dimensions of those parts yield in sufficient buckling resistance [9]

3 Description of the improved numerical structural model

A numerical model that depicts the previously described geometry, was already developed using a general-purpose finite element software (ABAQUS). At the improved numerical model obtained in this thesis, the initial geometry and the loading conditions have remained the same, while extensive modifications on the finite element mesh quality and on the interactions between the components of the platform were performed. Those modifications boosted the computational efficiency of the model and made the solution process to converge. The improved numerical model is described below.

Every component of the platform, more specifically the OWC chambers, the column cylinders, the system of braces, the mooring lines, the conical cups, and the truss structures, were modeled as individual parts which are combined to form the total assembly of the platform.

3D reduced integration shell elements were used for the column cylinders, OWC chambers and braces, while 3D beam type elements were employed for the stiffeners of column cylinders, mooring lines and the truss structure that supports the OWC conical cups.

The column cylinders along with their interconnected braces and OWC chambers were merged, generating a new part that includes the combined geometry of the individuals Figure 22. Merged structure in the numerical model. It consists of column cylinders, braces and OWC chambers. The rest components of the total assembly were attached to that merged part using tie constraints. This practically means that the nodes existing at the shared boundaries between the different parts forced to have the same translational and rotational degrees of freedom so that continuity is established.

In the context of the specific analysis that will be implemented in our case, the key components that are required to develop a well-defined numerical model in ABAQUS, involve the definition of geometry of the structure, the properties of the materials used, the steps which are associated with loading history, the boundary conditions, the constraints, and the mesh. More details about those main sectors in the current model are given below.

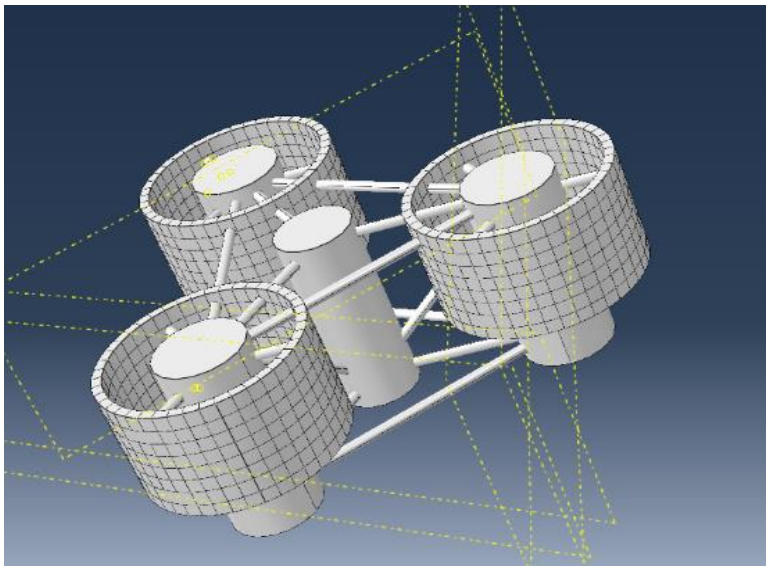

Figure 22. Merged structure in the numerical model. It consists of column cylinders, braces and OWC chambers

3.1 Steps

A basic concept in ABAQUS is the division of loading history in phases, called steps. In each step a different analysis procedure can be selected, depending on the nature of the applied loads. The current analysis is comprised of 4 loading steps and an initial step. During the initial step, the boundary conditions are applied to the structure. Through the first loading step the hydrostatic loads as well as the distributed loads that represent the ballast and the weight of the air turbines are applied to the model. Over the second step, the system is subjected to its own gravitational force which results in the stabilization of the platform at the desired draft of 20m below SWL. In those steps static analysis procedure was performed. In steps 3,4 dynamic implicit type of analysis was performed in a quasi-static application, which means that static loads were used but the moment of inertia of the structure was added to the solution algorithm. In such manner, higher convergence rates can be achieved compared to the static procedure and the stability of the solution algorithm is improved. The loading steps will be further analyzed providing a complete description of the exerted loads and the sequence which they are applied:

Loads at step 1:

During the first loading step, hydrostatic pressure is exerted on all surfaces that are submerged. Additionally, distributed loads that represent the ballast and the weight of the air turbines are applied. Ballast is any extra mass that is added on a floating structure to improve stabilization and to facilitate achieving the design draft. Changes in ballast mass affect the equilibrium between the weight and the buoyancy force of the structure and the pretension of the tendons. In the specific case of REFOS platform the ballast was calculated so that the platform is stabilized at the desired draft of 20 meters below SWL. In the numerical model, ballast is represented as distributed loads acting on the bottom surface of OWC chambers and as point masses acting on the bottom end of column cylinders.

Loads at step 2:

Gravitational force of the platform is exerted on all surfaces of the model, at the 2nd loading step. At the end of the 2nd step equilibrium between the weight of the structure and the loads that are included in the 1st loading results in the stabilization of the platform at the desired draft. Thus, the system is stabilized at the draft of 20m below SWL, and the platform is at the free-floating state.

Loads at step 3:

Loads that emerge from the operation of the WT, including moments come from rotation of the blades and the weight of the WT tower are applied to the platform during the 3rd loading step. They are exerted on the connection point between the platform and the tower, which is the top surface of the central column cylinder [Figure 23]. Those loads are expressed in terms of three maximum forces and moments that are transferred from the tower to the platform. They were calculated by the NTUA and represent the coupled hydro-elastic behavior. Those data represent the loading case that originates from the most demanding installation location, the region at the North Sea, in which the tougher environmental conditions occur (higher speed of winds and more intense waves compared to the locations on the Mediterranean Sea).

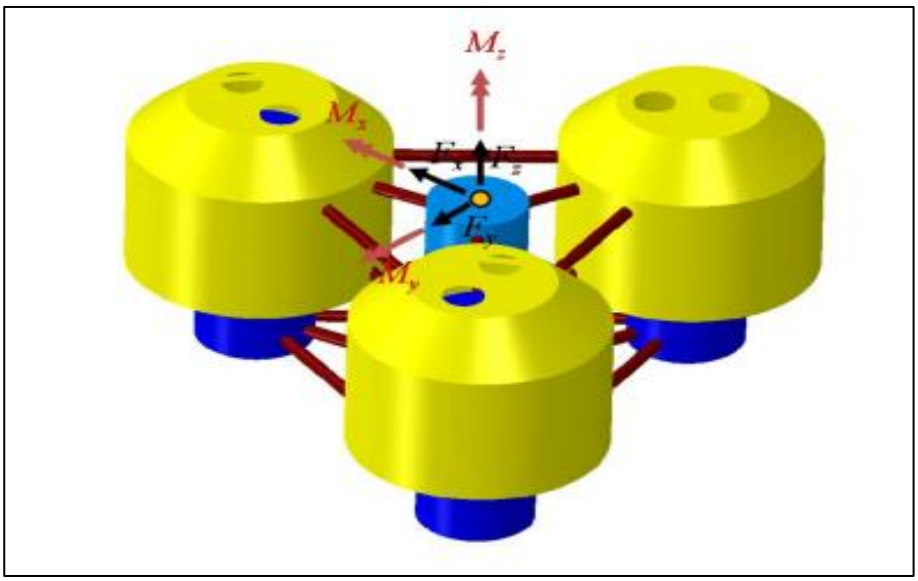

Figure 23. Maximum loads transferred from the wind turbine to the platform [12]

Table 5. Maximum loads transferred from the tower of WT to the platform

F_X (N)	48000	M_X (Nm)	$-5.335*10^8$
F_Y (N)	$5.5*10^6$	M_Y (Nm)	-23400
F_Z (N)	$-1.61*10^6$	M_Z (Nm)	$-1.19*10^7$

Loads at step 4:

During 4th loading step the extreme hydrodynamic loads from the combined action of sea currents and waves occurring during a storm are transferred to the platform making it the most demanding loading case. The values obtained represent the location 3, North Sea. Since those loads are greater in L3 due to local environmental conditions the loading step 4 is the worst-case scenario. Those loads are the maximum pressures that are exerted on the submerged surfaces of the platform. The maximum provided pressure was 92.31 MPa. [12]

The extreme hydrodynamic pressures at the inner and outer surfaces of the OWC chambers and for the external surfaces of the column cylinders were calculated by NTUA. Those extreme wave states correspond to a 50-year return period duration. [10], [11]. By using a CFD analysis which simulates the interaction between these wave states at the corresponding frequencies and the geometry of the platform, the loads that were generated on the submerged surfaces of the platform were obtained. The provided data were the pressure at different points with respect to depth and angle, around of each cylindrical surface (OWCs and column cylinders). More specifically

those values were evaluated at points of the above surfaces that differ 1m along Z axis and π/16 rad in angular direction. Those values are not in the appropriate form to be directly imported to ABAQUS interface, as they represent point loads that result in a non-uniform pressure distribution.

DLOAD is a specific type of an external subroutine that is imported to ABAQUS aiming to describe the variation of a non-uniform distributed load as a function of spatial and time parameters [2]. In the present case DLOAD subroutine was used to define the hydrodynamic pressures on the submerged surfaces of the platform as a function of position.

In the DLOAD subroutine used for the specific numerical model, a simple but essential methodology is implemented for the conversion of the point loads to distributed. The previously described data of pressure at the submerged surfaces of the structure, are contained in tubular form inside the subroutine. By applying linear interpolation between the values of pressure of successive points in two directions, along the Z axis and along the circumferential direction, the required pressure distribution is obtained. DLOAD subroutine is then imported to ABAQUS and the spatial variation of the maximum hydrodynamic pressure at the surfaces of the platform is obtained.

3.2 Boundary Conditions:

The main boundary conditions describe the seabed. Seabed and more specifically the anchors that are attached in the seabed, are modelled using an 'ENCASTRE' boundary condition (BC) which means that the translational and rotational degrees of freedom are fixed. The lower end of the tendons of the platform is connected to the fixed boundary through the special connector elements that allow only a maximum relative rotation of 10 degrees before locking, while constraining the translational degrees of freedom.

A temporary BC is used during the first 2 loading steps that allows only the vertical displacement of the structure and prohibits rotation about Z axis, so that the platform will translate only in the Z axis reaching the desired depth of 20 m below SWL. After the platform stabilizes at the projected draft, those boundary conditions are deactivated. Thus, during the loading steps 3 and 4 the only active BC is the fixed connection to the seabed.

3.3 Constraints

Constraints in general are used in Abaqus to constrain partially or fully the DOF of a group of nodes of the structure and couple their motion to the motion of other nodes. There are several types of constraints in ABAQUS depending on the application. In the current model, the different parts joined together using TIE CONSTRAINTS. A TIE constraint joins two separate surfaces that are sufficiently close together permanently, so that no relative motion occurs between them. This is done by

Tie constraints are used to connect the rest of the assembly to the merged structure that is depicted to figure 1. Therefore, there the following tie constraints have been used:

- Tie between bottom surface of conical casing of OWC device and truss structure
- Tie between truss structure and top surface of OWC chambers
- Tie between stiffeners and internal surfaces of column cylinders

Applying the right constraints to a numerical model is crucial for the convergence of the analysis, since letting a specific part unconstraint could cause unexpected behavior of the solution. Numerical singularities could occur, meaning that a region of the structure sustains rigid body motion. This issue causes major convergence problems and invalid results. To prevent rigid body motion in a static analysis adequate boundary conditions and constraints should be provided. Additionally, inadequate definition of constraints could cause penetration between parts of the model that are initially in contact. Unexpected penetration is another issue that causes convergence problems.

Special connector elements

ABAQUS interface contains several tools to model, the actual connections between parts, such as hinges, joints, and springs. Connector elements that belong to the general category of connections are used to simulate the actual arrangements described at Figure 20 that are attached to the upper and lower ends of tendons allowing a relative rotation of 10 degrees. After that value is reached, those connectors are set to constrain all the available rotational DOF. At Figure 24, the location of the connector elements in the total structure is illustrated. They have been employed 2 connector elements for each mooring line, resulting in a total number of

12. Connector elements are essential for the analysis, as they provide the required rotational flexibility of the platform.

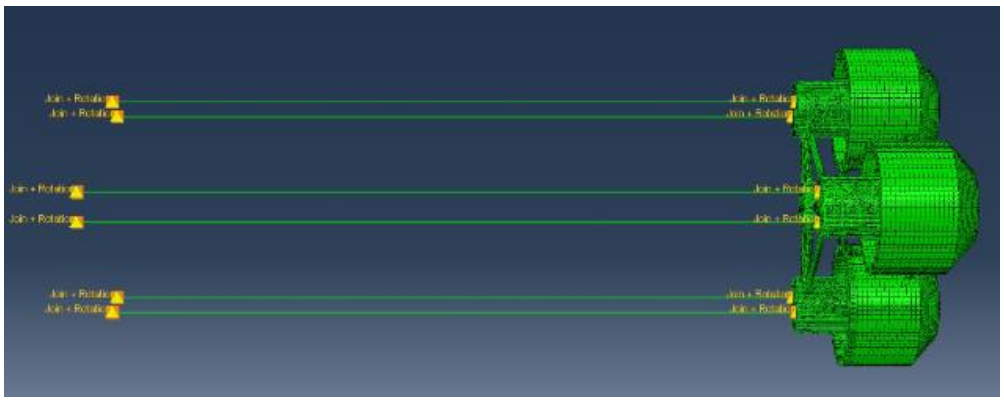

Figure 24. Location of special connector elements at the numerical model. Those elements join tendons with anchors and platform hull, while allowing relative rotation of 10 degrees.

3.4 Mesh

3.4.1 Mesh optimization process

The poor quality of mesh is a main reason for increased computational cost and divergence of solution process. A large-scaled enhancement of the finite element mesh of the already developed numerical model was performed, aiming at boosting its computational efficiency and making the solution algorithm to converge. The overall phases of the mesh optimization process are described below. The first phase was to establish a uniform mesh with a reduced number of elements compared to the initial model. Subsequently, the shape and quality of elements was enhanced in all surfaces, so that the computational cost diminishes, and a successful simulation is obtained. By interpreting the first results of simulation, regions that needed a denser mesh were located. Denser and more detailed mesh was employed in region that appear to withstand higher stresses while a lighter mesh was applied to surfaces that contained lower stress concentration factors. Then, again the new generated mesh had to be verified about the shape and quality of elements and a new simulation had to be performed to determine if a smoother stress distribution was acquired. This iterative procedure was followed until the desired stress field was acquired.

Phase 1

To reduce the number of elements, their average size was increased at all surfaces of the model. To obtain a discretization with a uniform mesh, the regions with complex geometry had to be manipulated. Partitioning tools of ABAQUS facilitate the process of splitting relatively complex surfaces to simpler ones. Furthermore, by applying mesh controls, meaning that by controlling the way that the elements are arranged around a surface, discretization became smoother.

Phase 2

The next step was to examine each surface of the total model thoroughly and locate the elements with poor shape that were distorted. Distortion of elements limits the computational efficiency, as the solution algorithm struggles to obtain equilibrium between internal and external forces, when an element has a problematic shape. Local improvements of mesh quality, especially in regions with complicated geometry were necessary. In every region that is around a circular surface, like the region of the OWC chambers which is crossed by the braces, the aspect ratio of elements was bad. Applying denser mesh and using different type of elements such as the 3D triangular shell elements (S3) which fit better to more demanding geometries such as the elliptical openings of the OWC stiffeners illustrated at *Figure 25*, was a successful way to limit the distortion. This procedure was done iteratively in all surfaces of the platform with problematic discretization. Eventually, a much smoother mesh with elements having the appropriate aspect ratio was acquired. The above changes boosted the computational efficiency of the model.

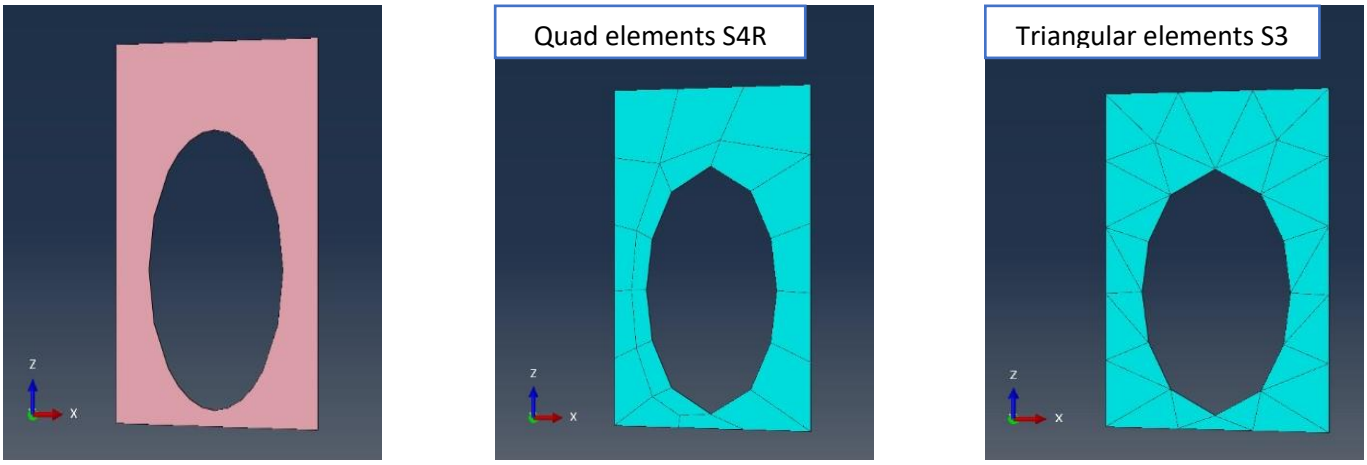

Figure 25. A part of vertical OWC stiffeners (left configuration) is modelled with quad and triangular elements. Quad elements are distorted when applied around circular geometries (middle configuration) while triangular elements fit better to the same geometry (right configuration).

Phase 3

Once the mesh quality improved and the simulation was successful, critical regions of the structure were determined by examining the results of the analysis. In those areas higher concentration factors with an erroneous stress distribution occurred and a further optimization of mesh was essential to obtain more reliable results. Thus, denser mesh was applied to those areas while coarser mesh was deployed to regions with less interest, meaning those which are loaded less and subjected to lower stresses. Critical regions were mainly the connections between braces and cylinders. This procedure has been done progressively with the ultimate target to achieve mesh convergence. According to that process, the element size is decreased gradually aiming to establish a more reliable stress distribution. To ensure mesh convergence to the critical regions of the structure, 3 identical models were created with a gradually increasing number of elements at the vicinity of critical regions. The effect of that successive remeshing to the stress field is described in chapter 4.

3.4.2 Element types that were used for the analysis

All element types that were used in the model account for stress/displacement analysis. More specifically, 3D reduced integration shell elements (S3, S4R) were used for the braces, the column cylinders, the conical casing and the OWC chambers, while 3D beam type elements (B31) were used for the stiffeners of cylinders, the mooring lines, and the truss structure.

The symbol S3 describes a linear 3-node triangular element, while the S4R stands for a linear 4-node quadrilateral element [Figure 27]. The above element types define general-purpose conventional shell elements which account for finite membrane strains and arbitrarily large rotations. Thus, they are appropriate for large-strain analysis.[1]

The beam type B31 elements stand for two-node linear line elements. They are depicted at Figure 26. Those elements use linear interpolation and follow the Bernoulli-Euler approach with the addition that allow transverse shear strain, which is a characteristic of Timoshenko beam theory. Thus, B31 elements are formulated so that they are efficient for both thin beams, where the Bernoulli-Euler approach is more accurate, and thick beams in which Timoshenko beam theory fits better. [1]

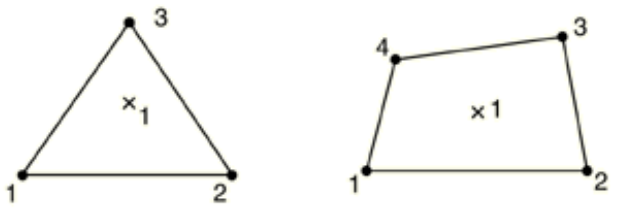

Figure 27. Shell elements. S3 type on the left and S4R type on the right. Both types of elements have one integration point. [2]

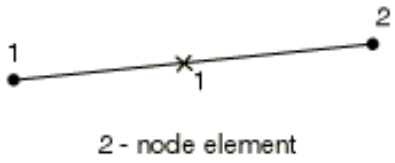

Figure 26. Beam type B31 element with one integration point. [2]

The outcome of the previously described mesh optimization procedure was a numerical model with an initial mesh containing 148097 elements and 127343 nodes. More specifically the spectrum of elements consists of 62432 of B31 type, 62845 of ST4R type and 22820 S3 type elements. In Figure 28 the initial optimized mesh is illustrated, for the total assembly of the model.

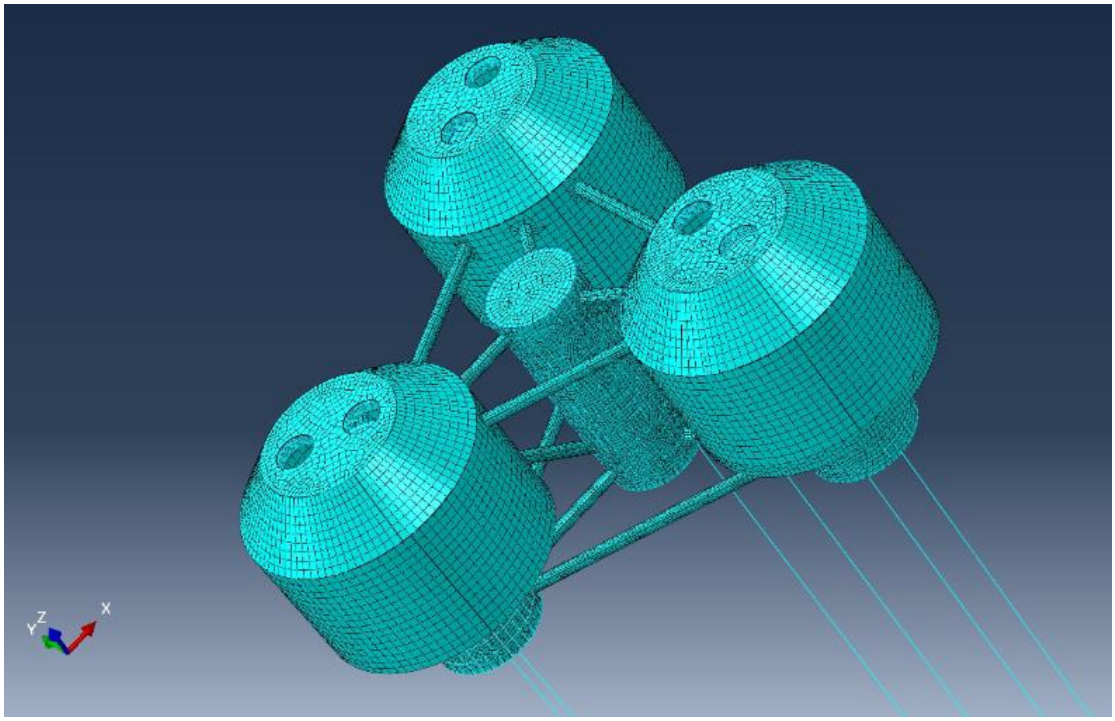

Figure 28. Initial mesh of the model. It consists of approximately 148000 elements in total.

Considering that the critical points of the structure would be the connections between cylinders and braces, that initial mesh was successively become denser around those regions. To illustrate the changes in the mesh density that was performed, the following figures are provided. In the next figures the central cylinder has been isolated from the total structure and the gradually denser mesh at the vicinity of connections between cylinder and braces is illustrated. In Figure 29 the initial mesh of the model is depicted. The nodes along the circumference of the connections are spaced with 0.3 meters distance from each other. The next figure, Figure 31 depicts a denser mesh compared to previous figure and the distance between successive nodes was reduced to 0.1 meters. The final figure represents the optimized configuration in which the distance between the corresponding nodes is 0.06 meters. Remeshing was crucial for the course of analysis since not only made the model functional and computationally efficient, but also it contributed to achieving more reliable results at the interesting points of the structure. The effect of the focused remeshing around the connections between cylinders and braces on the optimization results of the simulation is illustrated on chapter 4.

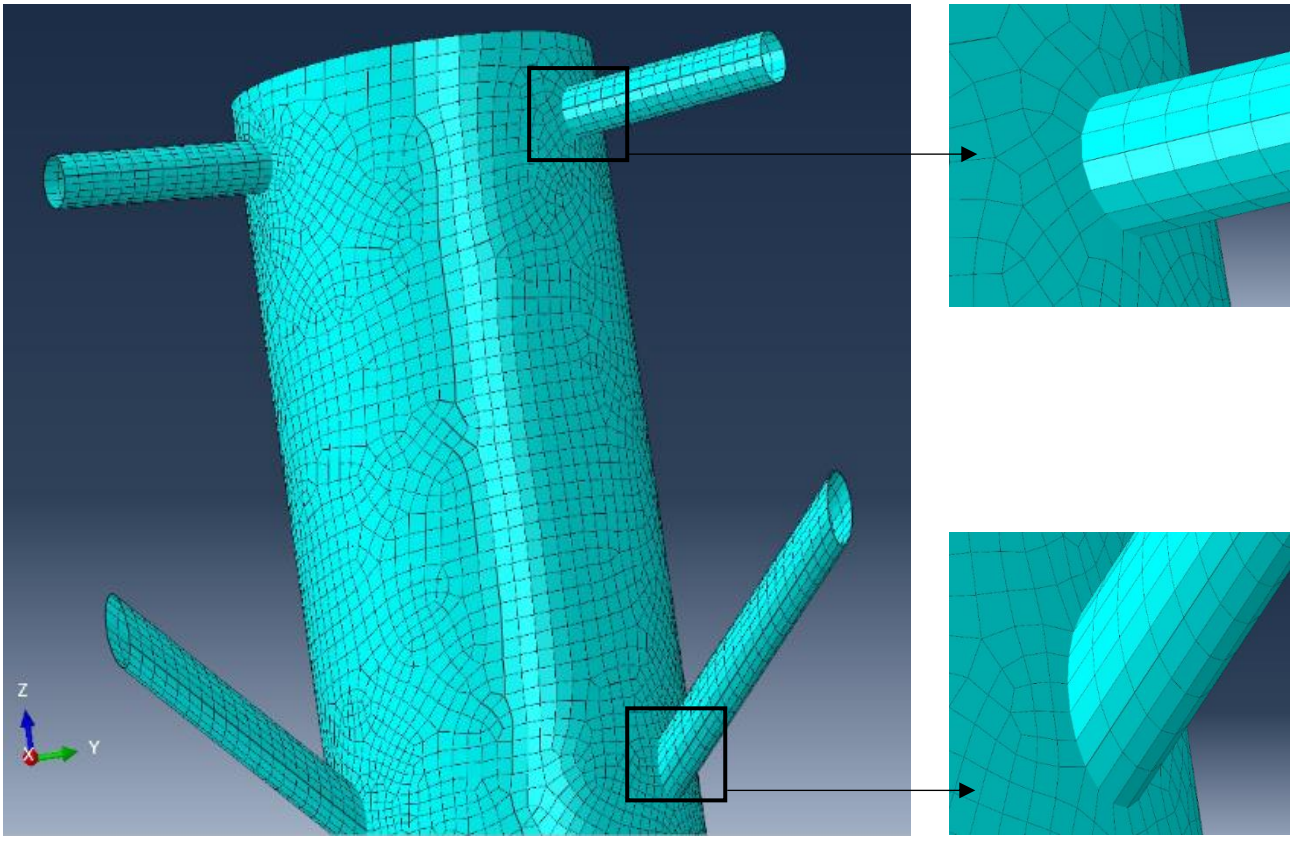

Figure 29. Initial mesh around connections of the central cylinder

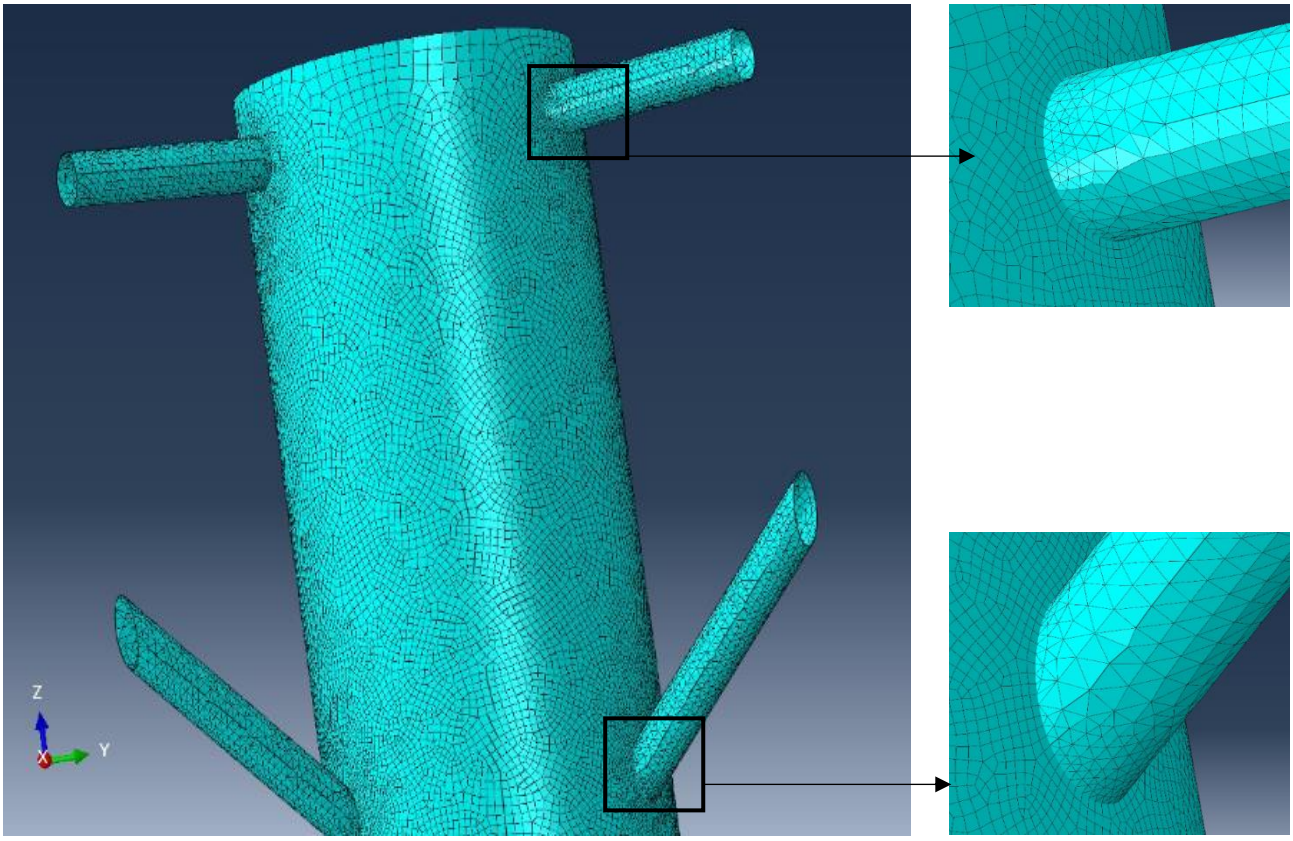

Figure 31. Denser mesh at the connections on the central cylinder

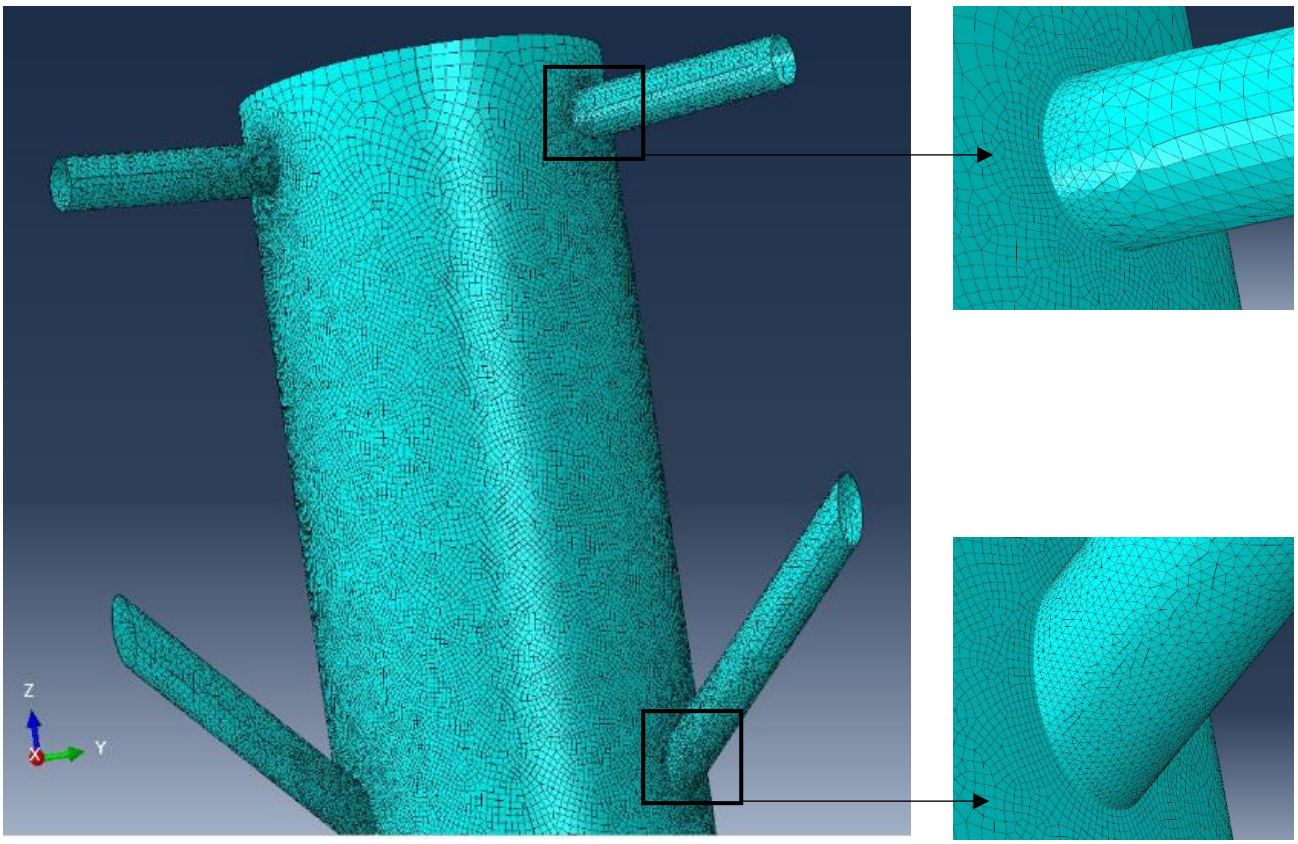

Figure 30. Final mesh around connections of the central cylinder.

4 Results of simulation

Following the basic finite element solution process, ABAQUS computes the nodal displacements of all nodes of the structure with a specific iteration method. Starting from nodal displacements, a numerous set of variables can be calculated by ABAQUS, the most common of which include stresses and strains, reaction forces and moments, and rotations. In the specific case of REFOS platform, the most representative results of the global response are the displacement of the platform and the stress distribution in the critical regions of the model. It is expected that the critical regions will comprise the sections where a low diameter ratio (minimum diameter over maximum diameter) is observed. That occurs in the connections between column cylinders and braces. Indeed, as it will be evident from the graphs below, the highest local stresses on the structure are detected in those areas.

Firstly, contour plots displacement at different parts of the structure will be evaluated, which represent the global response of the structure when it is subjected only to the static loads (gravity, hydrostatic pressure, and ballast). Subsequently, equivalent plot states will be presented for the end of the analysis step 4 (end of simulation) which includes the combined effect of all applied loads, which are dominated by the extreme hydrodynamic pressures. The upcoming values of stress will be compared to each other, and they will be interpreted to estimate the location of critical points of the structure.

4.1 Contour plots of displacement

At this point, information about the general displacement of the total structure is provided. A design consideration of the platform is to remain still in the vertical axis (Z axis), while allowing small offsets in lateral motion. The displacement path of the platform on the course of the subjected loads is illustrated in the following figures. The values on the legend of the figures are in meters. Initially, the figures focus on the magnitude of displacement through the steps of the analysis. The magnitude includes the values of the displacement at all three directions. The maximum value of displacement magnitude increases constantly, starting from a value of 40 mm after the hydrostatic loads [Figure 32], to a value of 230 mm after the loads transferred from wind turbine (step 3) [Figure 33]. Finally, it becomes 930 mm, which is the highest value of displacement through the analysis, which occurs at the end of the simulation [Figure 34]. Because of the great dimensions of the structure, even the highest displacement of 930 mm is not visible from Figure 33. To illustrate the motion of the

platform during analysis more effectively, the displacement will be scaled with a value of 60. The following figures [Figure 35, Figure 36] are analogous to Figure 32 and Figure 33, with the difference that the visible displacement is depicted as 60 times bigger. The initial position of the platform is also visible with grey color, so that the reader realizes the motion of the platform.

It is necessary for the safe operation and the stability of the WT that the displacement along the Z axis is close to zero. Even from the figures with the scaled response, it is visible that the displacement at the Z axis is significantly lower from the lateral displacement. To have a most quantitative approach about that issue, Figure 37 focuses on the displacement of Z axis or the U3. After the submission of hydrostatic loads, meaning at the end of analysis step 2, the max U3 displacement is 40 mm. The overall highest value of displacement at Z axis, is 110mm and occurs after the submission of maximum loas transferred from the wind turbine, at the end of analysis step 3. It is emphasized that this value appears at the extreme loading scenario. Thus, the design requirement of the platform to remain relatively still in vertical direction is fulfilled. If we compare that value with the maximum corresponding magnitude of displacement which is 930 mm, we realize that the lateral displacements of the platform are significantly higher than the vertical.

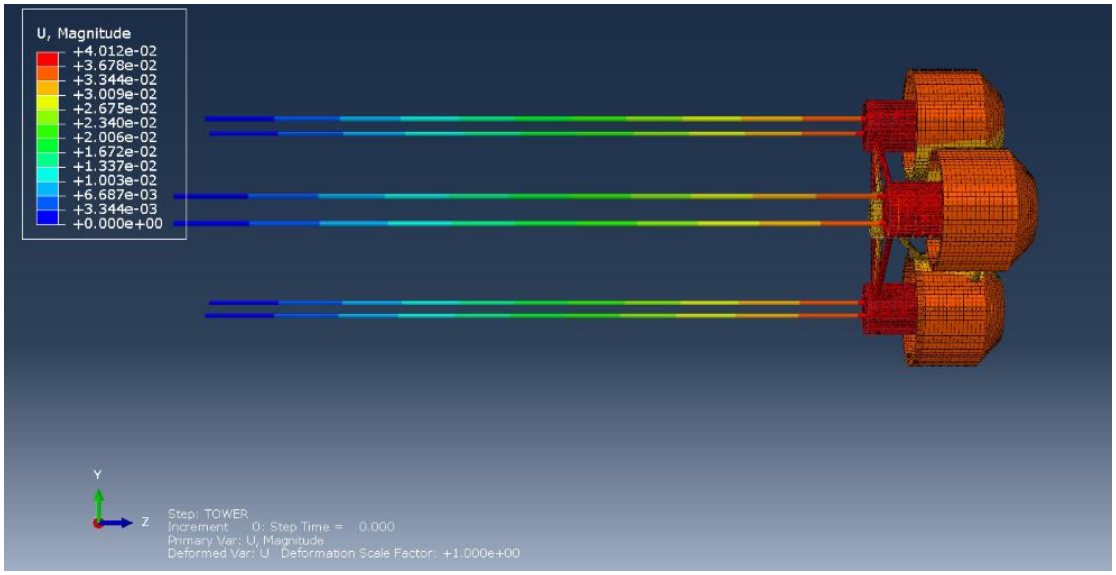

Figure 32. Magnitude of displacement after the submission of hydrostatic loads. As it is depicted in the legend, the maximum value is 0.04 meters.

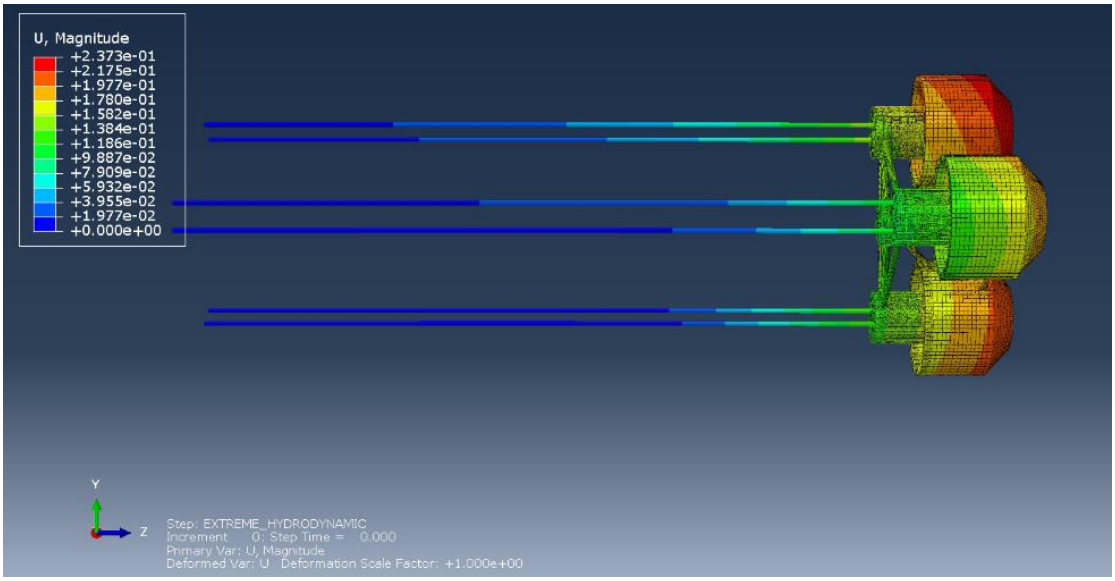

Figure 33. Magnitude of the displacement of the platform after the end of 3rd analysis step, during which the loads transferred from the WT to the platform are applied. The maximum value is 0.23 meters.

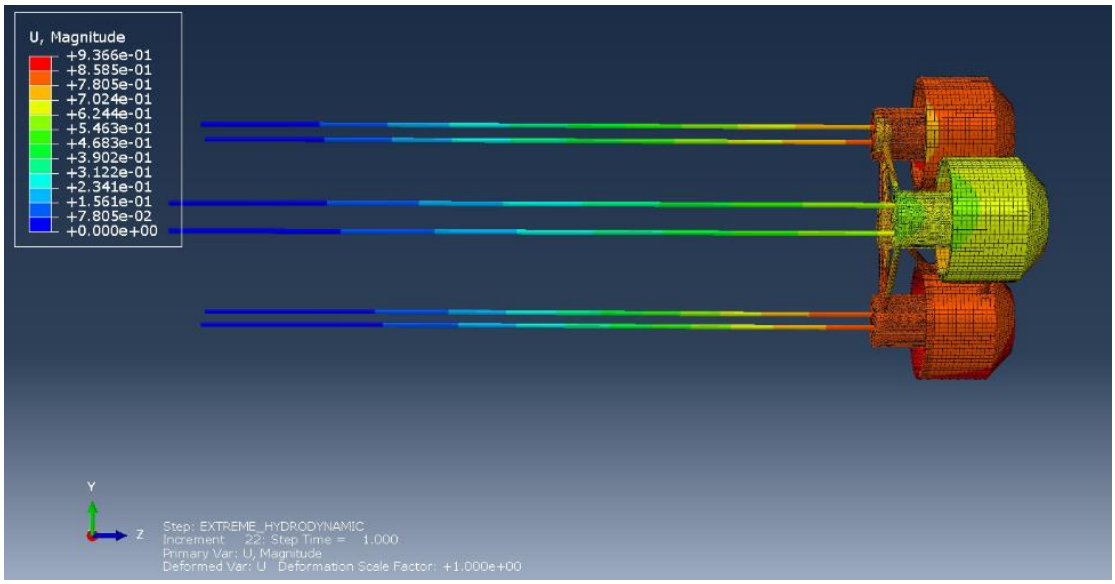

Figure 34. Magnitude of displacement of the platform after the extreme hydrodynamic loading conditions, which occur at 4th step of the analysis. The maximum value is 0.93 meters.

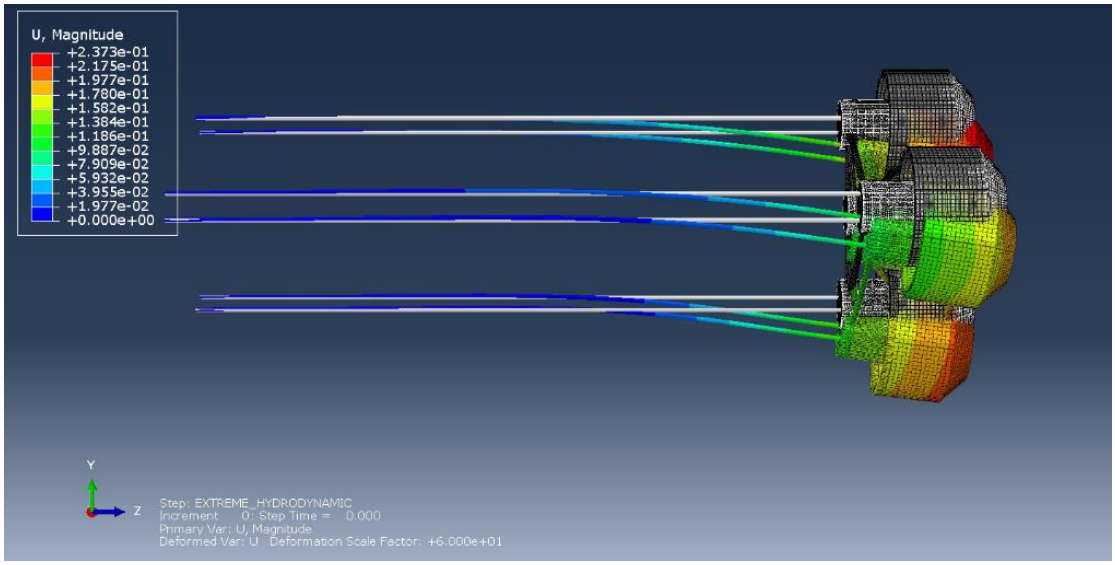

Figure 35. Magnitude of displacement after the 3rd analysis step. This figure is analogous with Figure 33, but the deformation has been scaled with a factor of 60. The grey configuration represents the initial position of the platform.

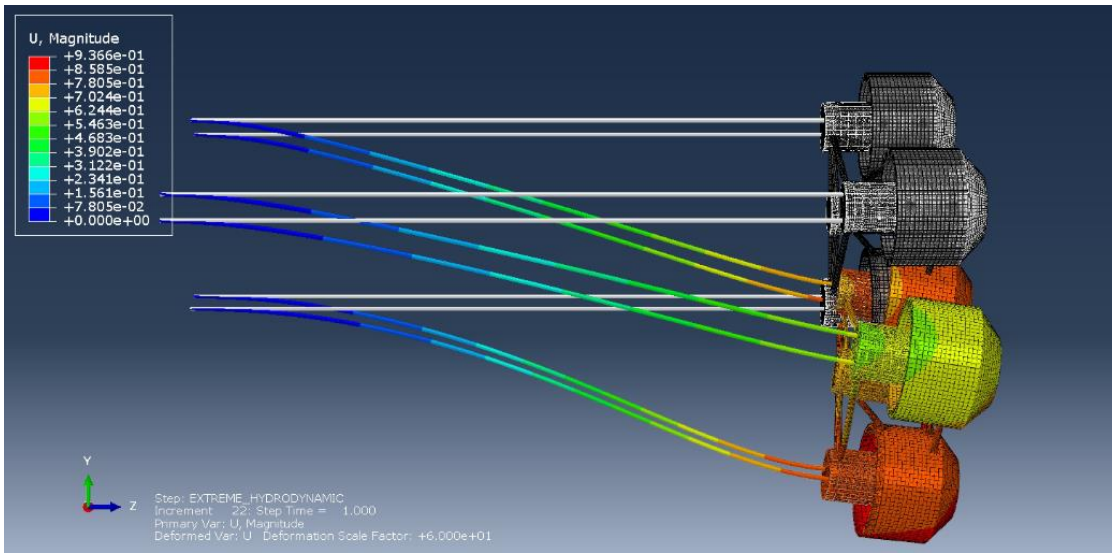

Figure 36. Magnitude of displacement of platform at the end of simulation. The figure is analogous with Figure 34, but the deformation has been scaled with a factor of 60. The grey configuration represents the initial position of the platform

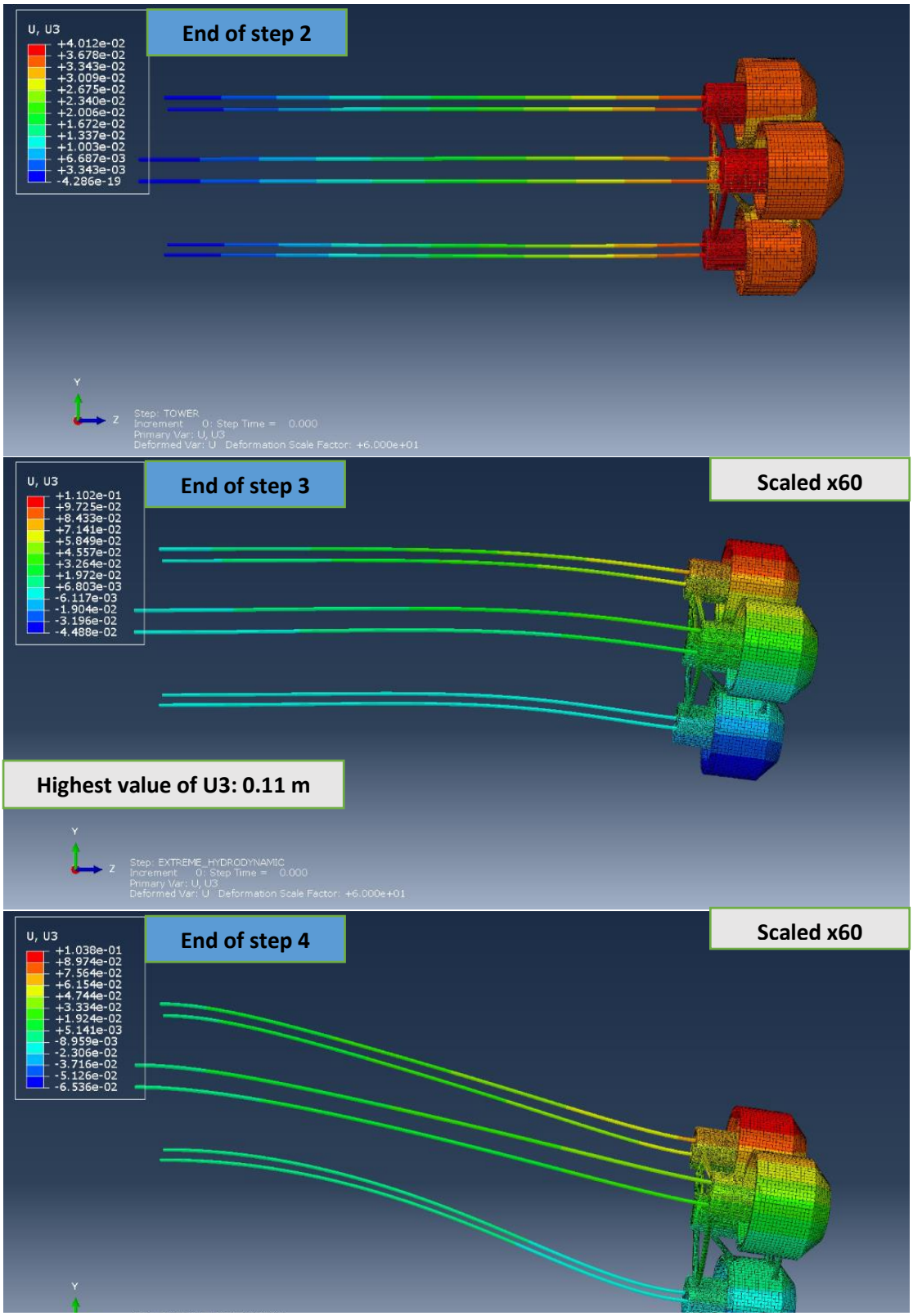

Figure 37. Displacement along Z axis of the platform during the steps of the analysis. The maximum value is 0.11 m which occurs at the end of the 3rd analysis step, during which the loads transferred from the wind turbine are applied.

Focusing on the maximum magnitude of displacement of the steel tendons depicted at Figure 38, the maximum value of 837 mm is obtained. The design requirements of the steel tendons of REFOS platform are to incur a maximum allowable offset of 5% of the water depth. Considering that the water depth is 200 m the maximum offset is 10 m. Thus, the value of 837 mm is totally in safe range. Furthermore, according to the right side of Figure 38, the tendons with the red color are stretched more the others. This is a consequence of the twisting motion of the platform which is visible from the Figure 36.

Thus, we should ensure that the global response of the system yields in the desired stress distribution around the critical regions of the structure. Global model is vital for the optimization procedure, but when it comes to the basic aim of this project which is the estimation of lifetime period of the structure, the local model must be formed since the failure mechanisms that will define the operation period of the platform is a local phenomenon that occurs at the vicinity of the critical regions. Therefore, the local model will provide a clearer interpretation of those issues. In the next figures, the stress contour plots are focused on the connections between braces and cylinders to illustrate the effect of optimization of mesh on the stress distribution.

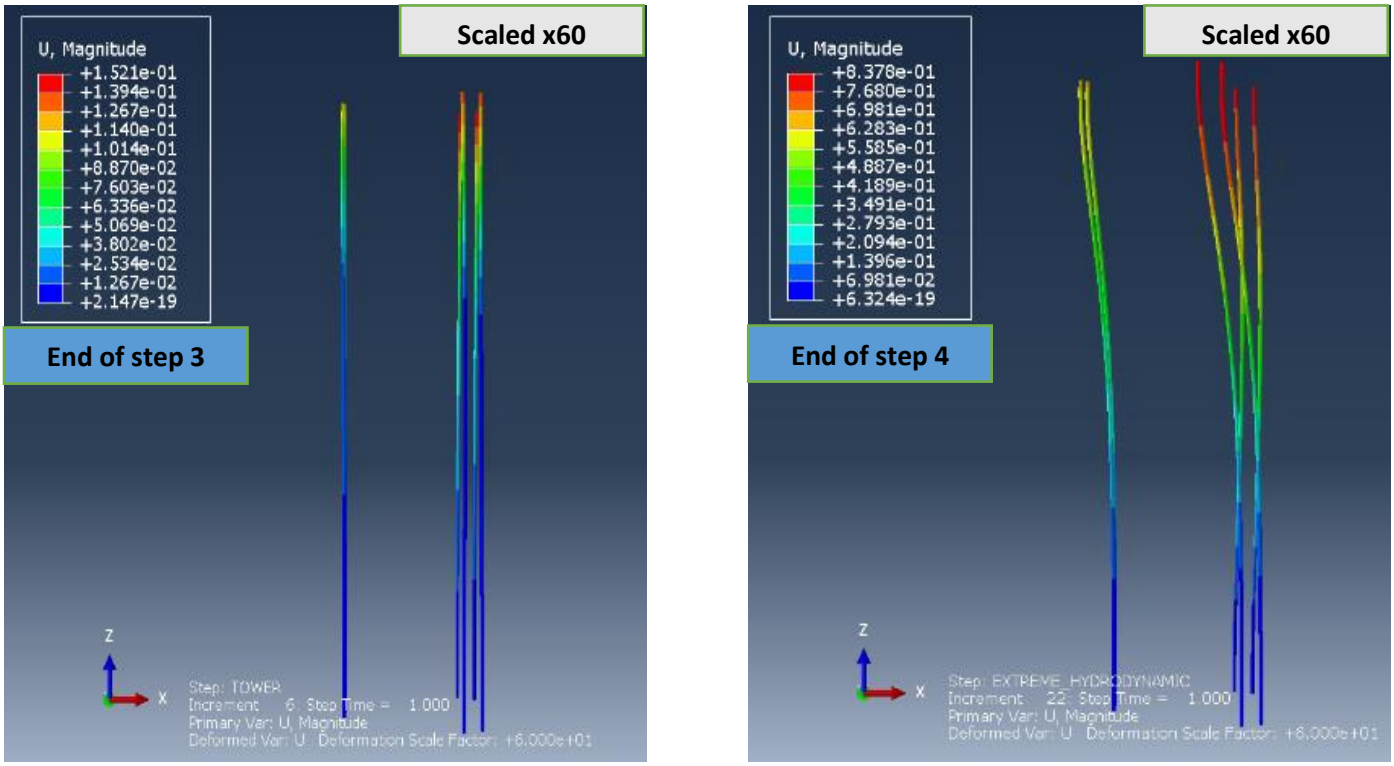

Figure 38.Maximum magnitude of displacement in tendons of the platform, after analysis step 3 (left) and after analysis step 4 (right) .The overall maximum values is 0.837 meters

4.1 Contour plots of stress

The provided values of stress at the legend of following figures are in Pa. To have a quantitative interpretation of the emerging values of stress, they are compared to the yield strength of the material which is 355 MPa for the S355 steel. It should be emphasized that linear analysis is performed, so the yield strength and the plastic path of each material has not been included in ABAQUS solver. The only material data that are provided is the mass density, the Poisson ratio, and the elastic modulus.

Stress distribution at stiffeners of column cylinders

As it is depicted in Figure 39 a) and b) the maximum stress at stiffeners starts at 28.56 MPa after the static loads and climbs to the value of 197.6 MPa after the extreme loading scenario, at the end of simulation. In terms of yield strength of the material this is translated to 8 % of σ_{yield} in the first occasion and to 55% of σ_{yield} at the extreme conditions.

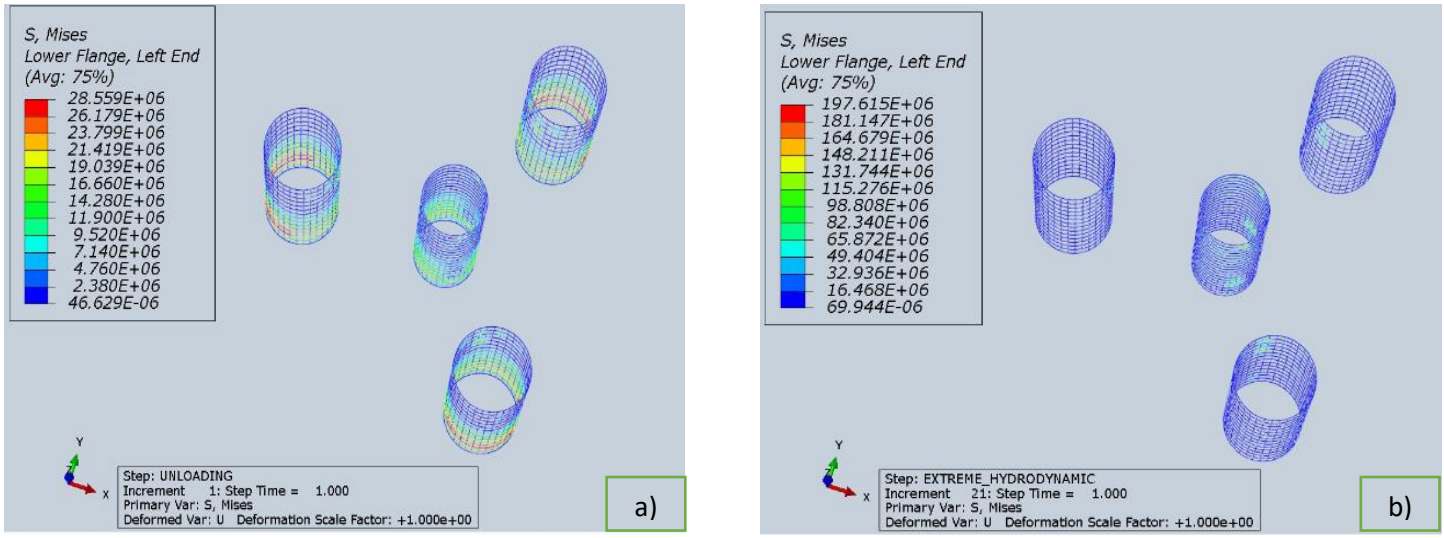

Figure 39. Stress field at stiffeners of column cylinders. a) After static loading b) After extreme loading

Stress distribution at OWC devices

As mentioned in previous chapters, OWC devices are comprised of the OWC chambers, the conical cup, and the truss structure. Stress distribution of all subparts of OWC devices is illustrated in the contour plots below.

Conical cups

As Figure 40 represents the stress generated at conical casings of the OWC devices are insignificant compared to yield stress, as the maximum value of 34.68 MPa is only the 9.7% of σ_{yield}.

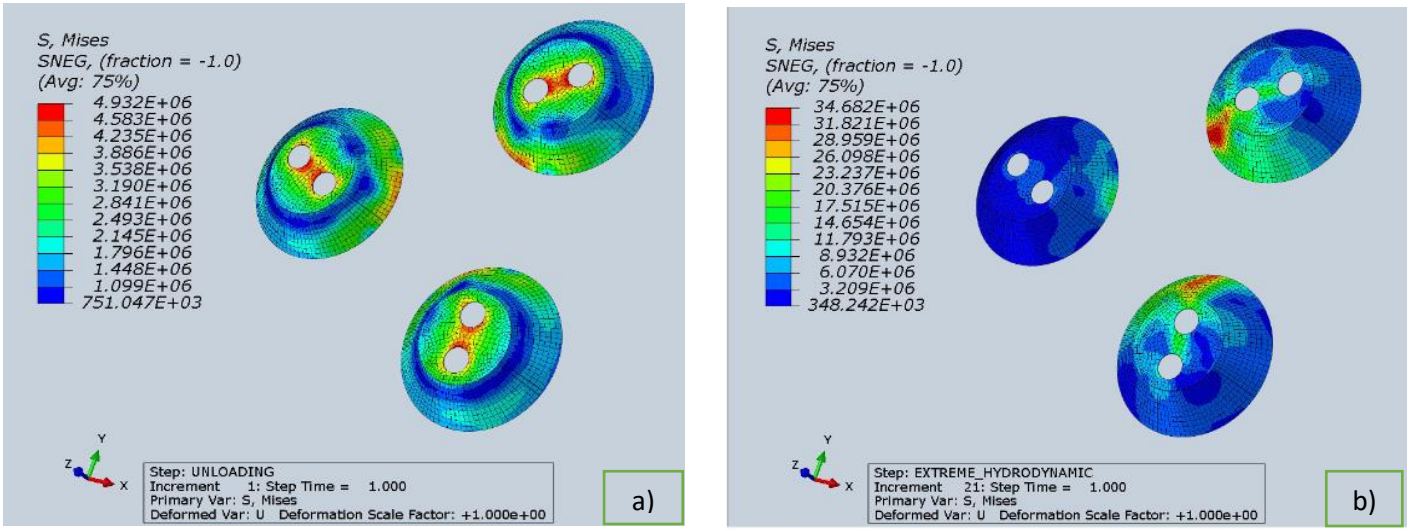

Figure 40. Stress field at conical casings. a) after static loading b) after extreme loading

Truss structure

About the truss structure, the maximum induced stress is 86.7 MPa, value which is minor compared to the yield strength of the material. The stress contour plot of the truss structure is illustrated in Figure 41. The left part depicts the induced stress field after the static loading, while the right part shows the response at the end of simulation, after the extreme loading case scenario.

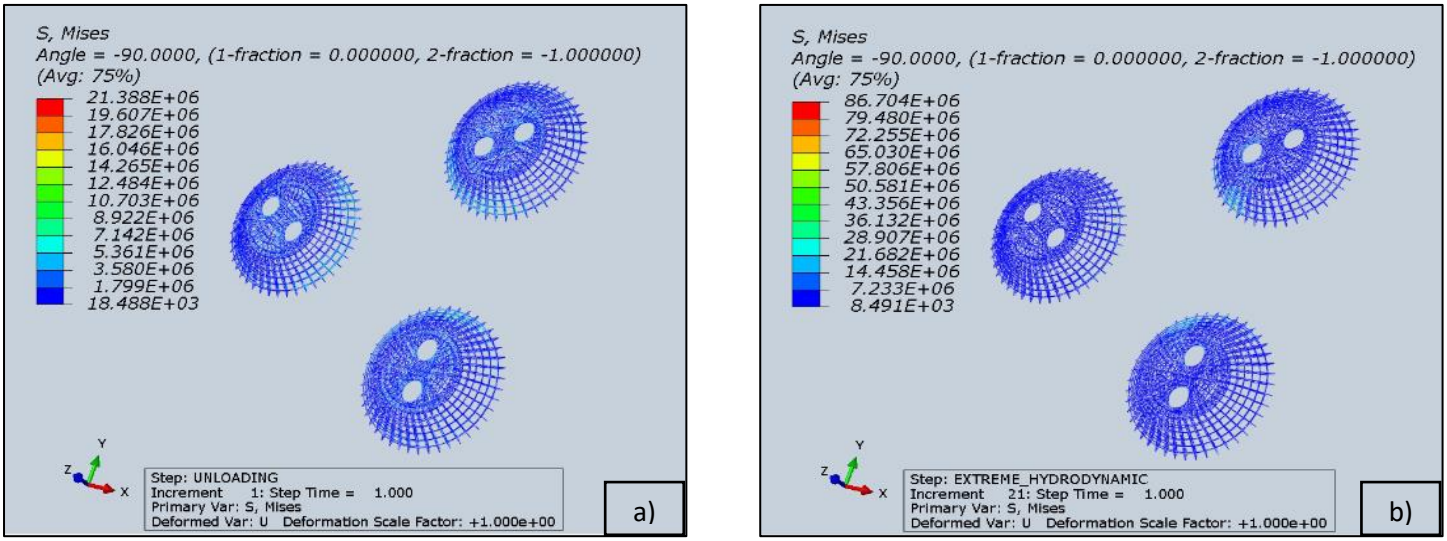

Figure 41. Stress distribution at truss structure a) after static loading b) after extreme loading

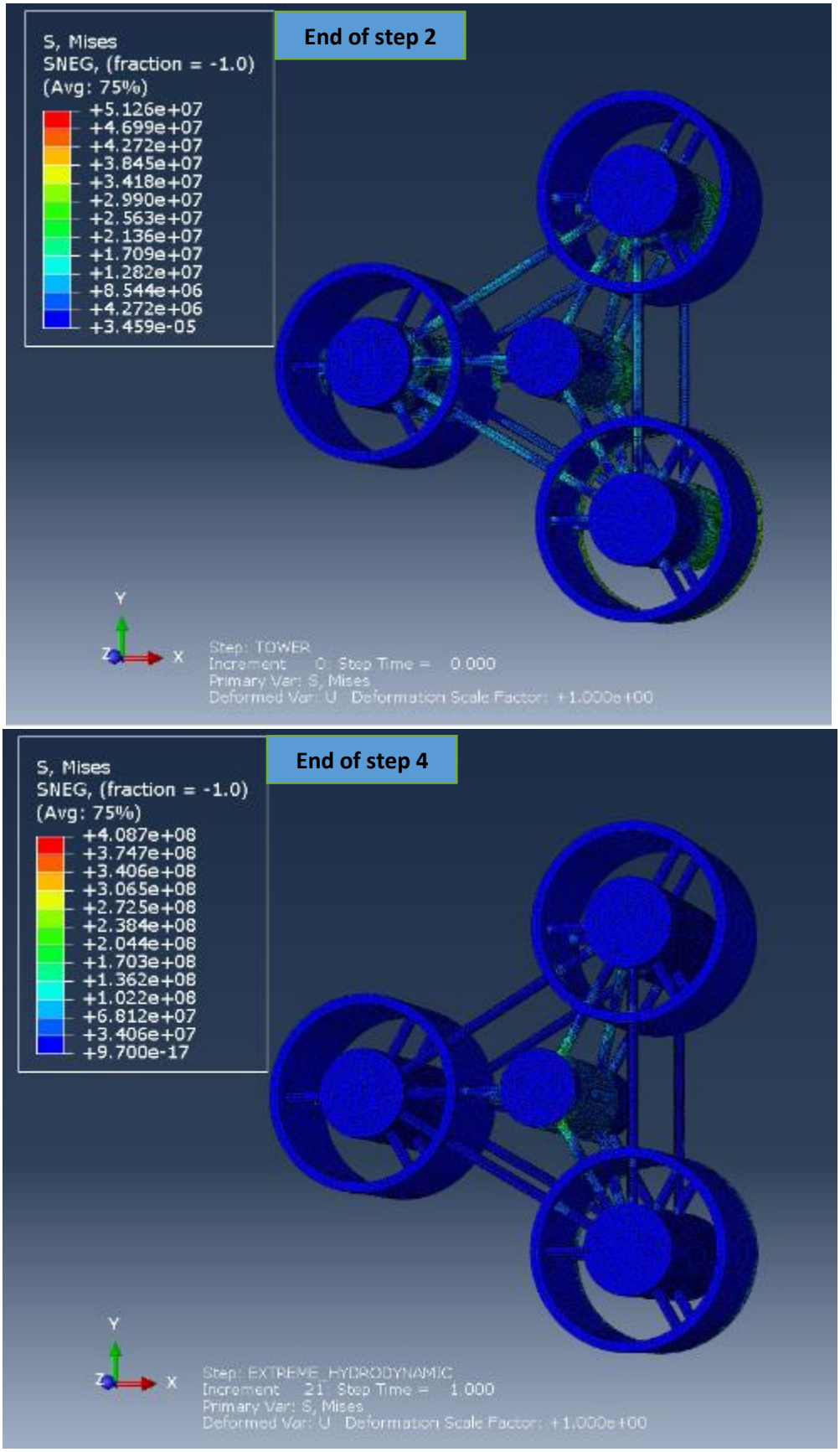

Figure 42. Mises stress on the triangular floater after the course of step 2 (top side) which includes the hydrostatic loads and after the step 4 (bottom side) which includes the extreme loading case scenario. OWC chambers are subjected to low values of stress on both occasions.

Examining the contour plot that is depicted at Figure 42, relative low values of stress are generated at OWC chambers. Thus, the OWC chamber, truss structure and conical cup of OWC device are structurally safe against yielding since they are in the elastic region of stress.

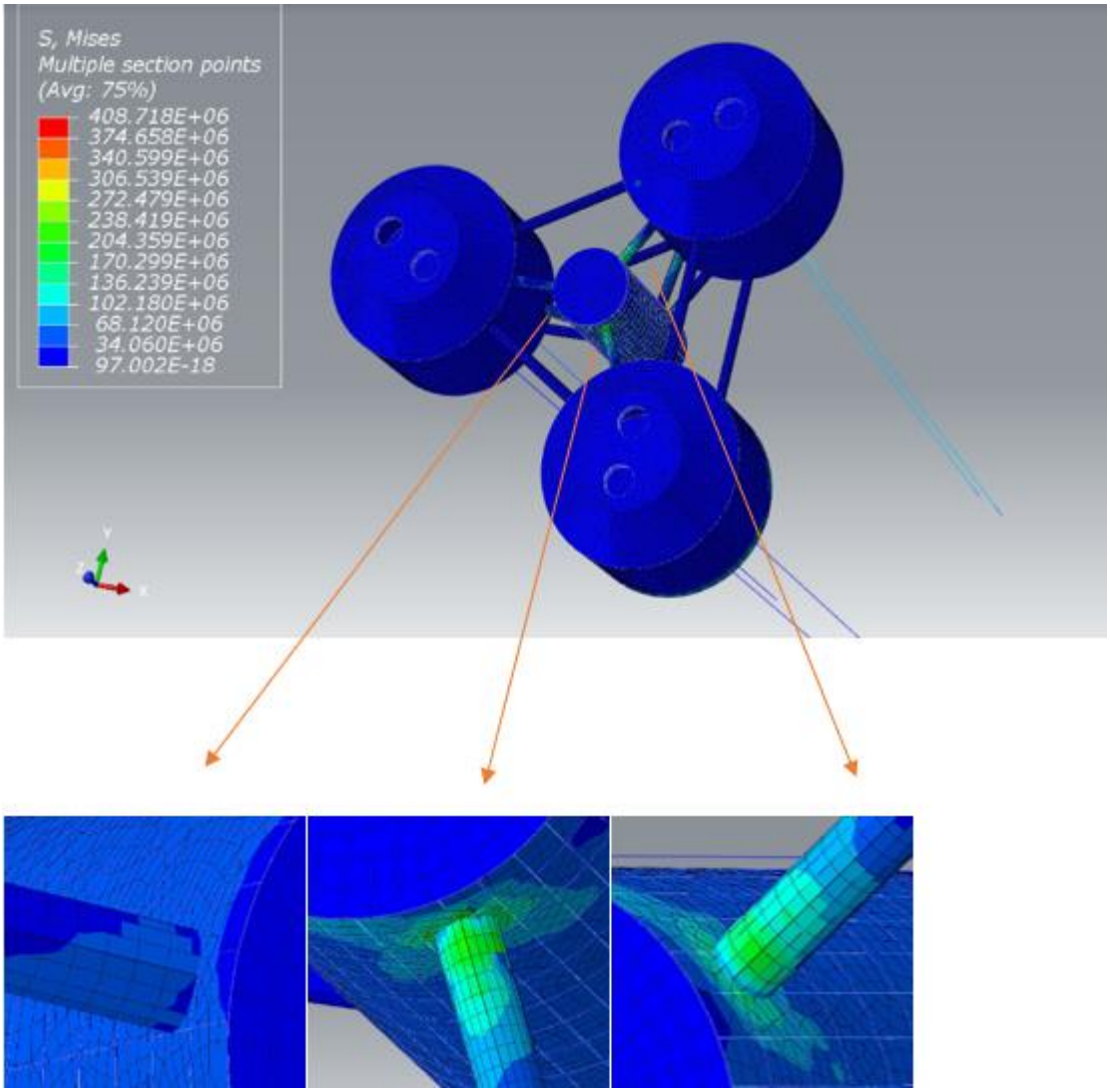

Figure 43. Connections with high concentration factors

At this point, having a clear depiction on how the stress is distributed on the whole structure, the location of critical points can be determined. As it is depicted in Figure 43. The regions where high stress concentrations are observed, constitute the critical regions of the platform, which are mainly the connections between braces and

cylinders. The stress field around those regions is important for the next phase of the analysis, which is the development of a local model that will include only the geometry around critical points. To achieve that, the stress field at the vicinity of those connections should be extracted and converted by integration to a 3D vector of forces and moments that will be used as the loading condition of the upcoming local model. This is the reason why several attempts for an optimized stress distribution around those areas of the model have been conducted, mainly by improving the mesh quality and mesh density at these points, as it was described in the «Mesh» paragraph of chapter 3. As smoother the stress field around the critical regions is, the loading condition and by extension, the results of the upcoming local scale analysis will be closer to real behavior.

4. 3 Focus on critical regions of the structure

From the Figure 43, it is visible that the connections in the central cylinder contain high concentration factors. Indeed, as it was stated at the beginning of the chapter, the critical regions of the structure are mainly the connections between cylinders and braces. To examine that issue more thoroughly a contour plot for the triangular arrangement of cylinders at the end of simulation is presented. By examining the Figure 44, stress concentration appears not only to the connections of central cylinder, but also to specific connections of the circumferential cylinders. It is evident though from the same figure that the side of CCC2 (Circumferential Column Cylinder 2) is less loaded that the others. This happens because the loads that came from the extreme hydrodynamic step have a certain direction since the waves cannot hit the structure from all sides simultaneously. There will be always one side that will be subjected to lower loads. In real conditions though, all connection points will be critical since the direction of the waves is not predetermined.

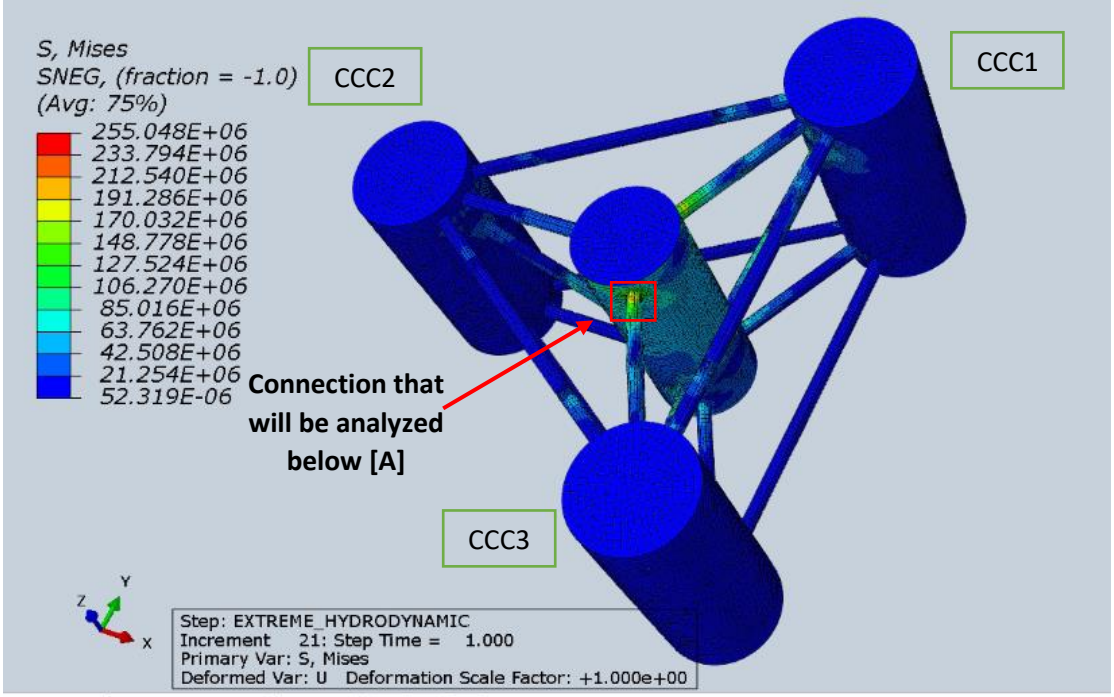

Figure 44. Stress distribution at the triangular arrangement of cylinders (floater). CCC→ circumferential column cylinder.

Aiming to obtain a smoother stress field around the critical regions, the size of elements around the connections was successively reduced. The outcome of these actions in the local stress distribution at one specific connection is depicted in the following figures. One among the critical regions of the structure, more specifically the joint between the upper part of circumferential cylinder 3 (CCC3) with the central cylinder [Connection [A],Figure 44], was isolated and the stress field in the vicinity of the connection was examined. As it is visible from the Figure 45, the induced stress field is relatively rough and the stress transition between consecutive elements is steep. This issue could be tackled by applying a denser mesh in that region. Two consecutive remeshings were established for that reason, and the acquired results are presented below. The following figures illustrate the effect of an increasingly improved mesh around the connection [A].

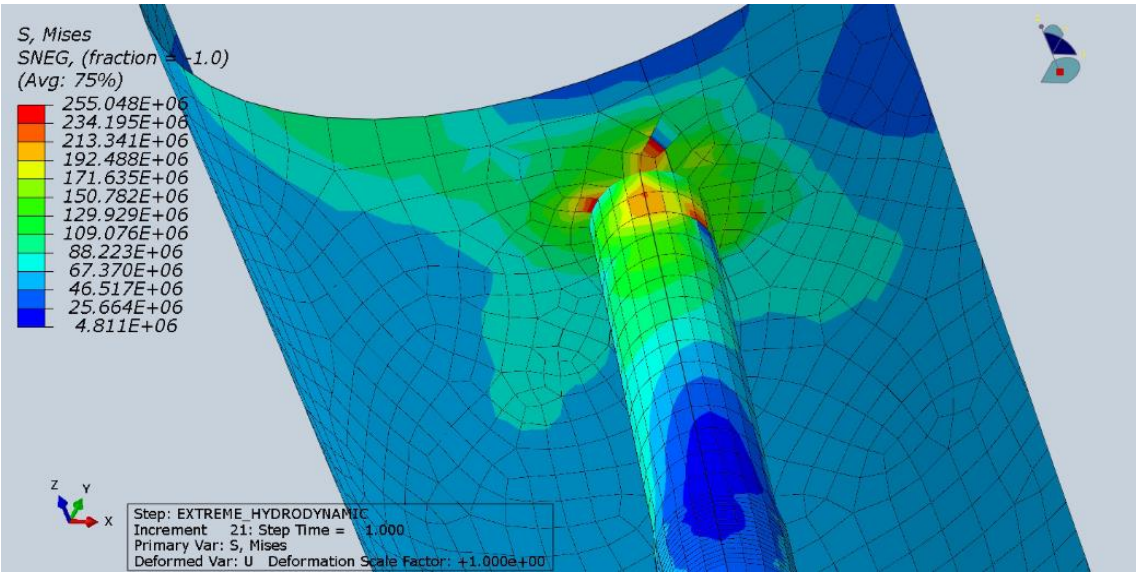

Figure 45. Stress field around the connection [A], obtained from the initial mesh. (Connection between central cylinder and circumferential cylinder 3)

The results of simulation after the 1st remeshing are presented in Figure 46. The initial mesh of Figure 45 has been improved yielding to an enhanced stress field. The stress distribution is smoother than the corresponding distribution of Figure 45, but there is still room for further improvement, as in the highlighted element of Figure 46, the transition of stress is quite steep making the stress field less reliable.

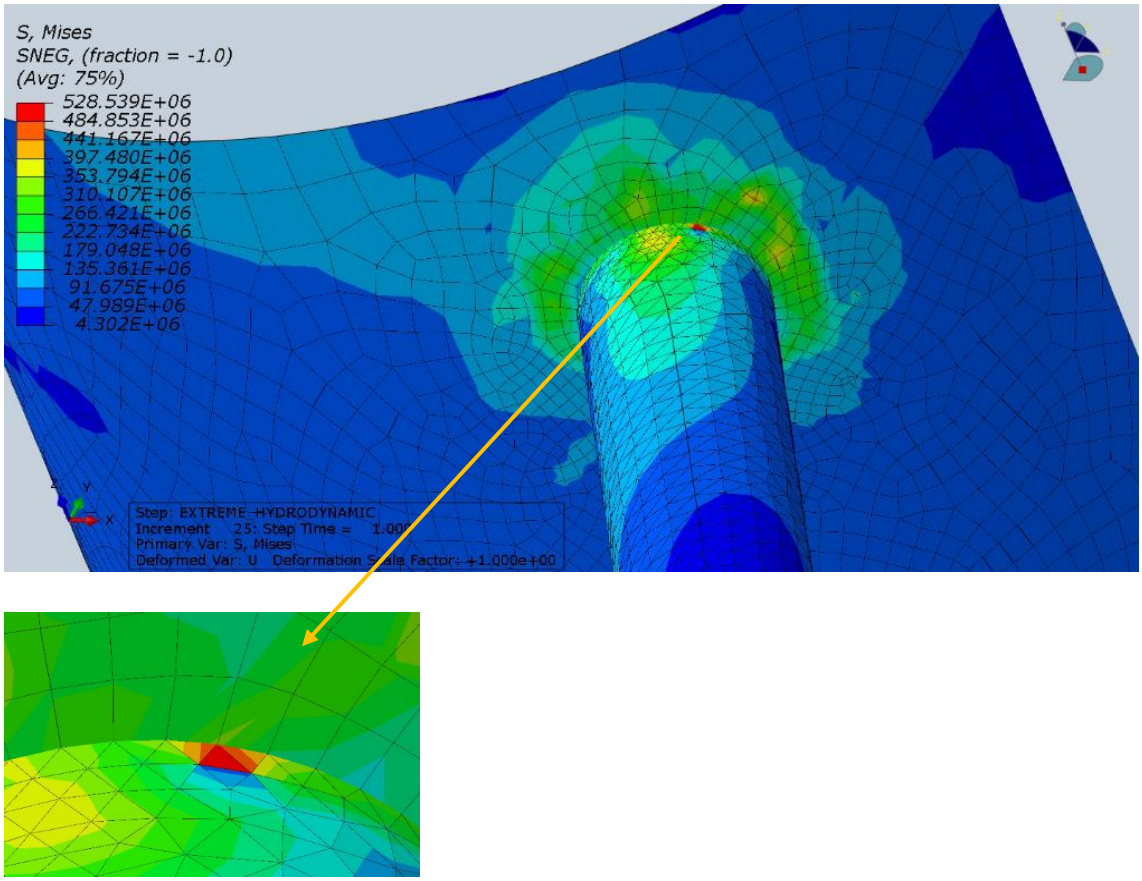

Figure 46. Stress field around the connection [A] after 1st remeshing.

Further increasing of mesh density was performed during the 2nd remeshing, and the stress distribution of Figure 47 was obtained. It's evident that the stress field is much smoother than both previous cases. Additionally, as it is depicted in the highlighted elements of Figure 47, the transition of stress values between consecutive elements is reasonable.

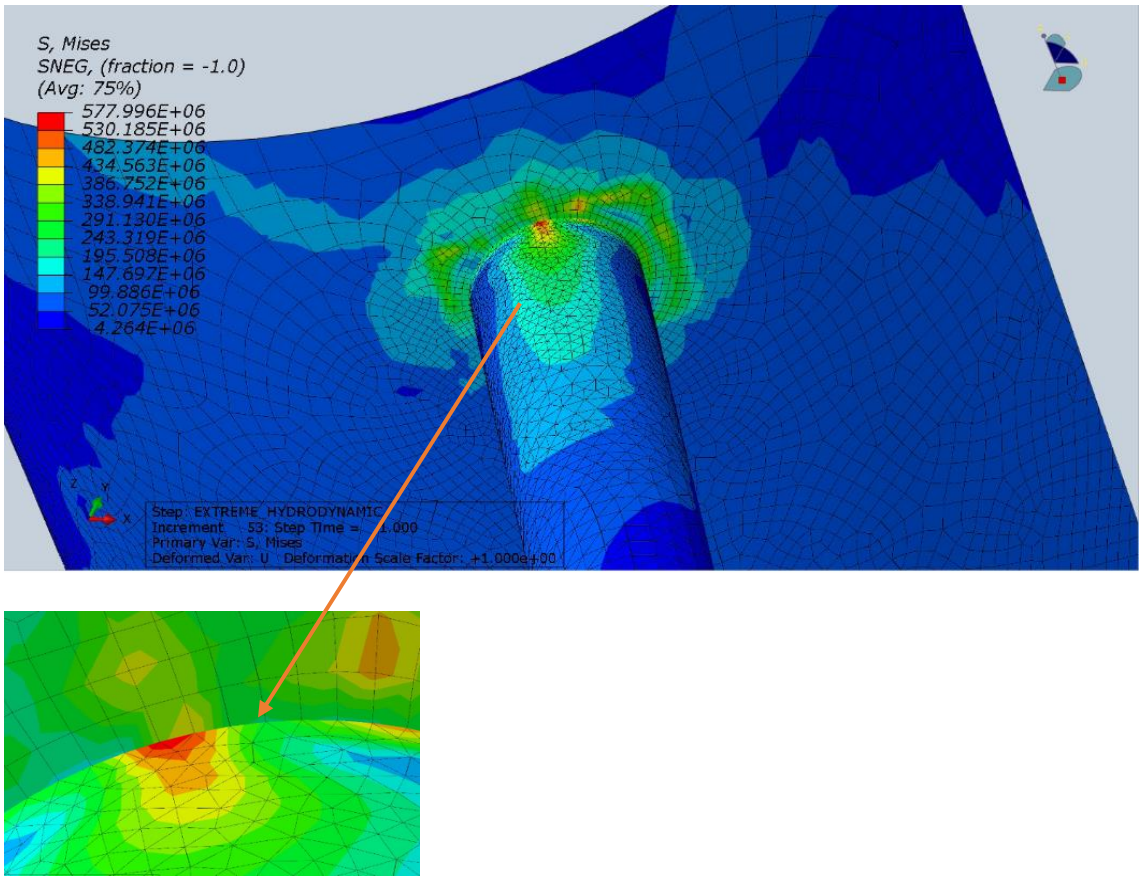

Figure 47. Stress field around the connection [A] after 2nd remeshing.

Despite that a sufficient stress distribution was obtained around the critical regions, if we focus on the magnitude of those stresses on the course of the above figures, we will realize that it develops an increasing tendency. The maximum values of stress field in the vicinity of connection [A] start from 255 MPa at the initial mesh and jump into the value of 578 MPa after the final remeshing. Thus, as the number of elements increases, the value of induced stress escalates. That occurs though only for the points very close to the connection. As it will be clarified in the next paragraph, this is an expected issue, and doesn't necessarily mean that plastic failure will occur. To proceed with the next phase of the analysis, we don't need the values of stress exactly at the connection, but the stress distribution in the region around. Thus, the escalating values of stress at the connections, doesn't affect the reliability of the analysis.

4.4 Interpretation of the obtained results

An important phase of the postprocessing of a numerical model is the interpretation of the acquired results. Most of the above presented results appear to be reasonable, with a major exception. The values of stress at regions that include intense changes in geometry, like the connections between braces and cylinders. The reason that lies behind that issue is the nature of the analysis that is performed. Elastic analysis is implemented for the simulation of the platform. An elastic analysis assumes that there is always a linear dependence between stress and deformation. This analysis while being computational effective it has certain limitations, especially when it comes to calculation of stress field between boundaries of connected parts. By increasing the number of elements, their average size and therefore their area decreases. Thus, an asymptotic rise of the computed stress occurs, and the corresponding values tend to infinity. Hence, this justifies the successive upsurge off stress values. If an elastic-plastic analysis was used, the same values of the stress would be much lower, since they would be limited from the plastic path of the material, which is not linear like the elastic analysis.

It should be emphasized though, that the values needed to proceed with the interpretation of the results and the next phase of the analysis, which is the future development of the local model, are not the stress exactly at the connections, but the stress distribution around them. This upsurge of the local values of stress despite being inevitable, it doesn't affect any part of the analysis.

When it comes to designing, the peak values of stress at the connections are never used. In fatigue analysis for instance, when it comes to the calculation of the geometric or hot spot stress at the weld toe, which in our case is represented by the connection between cylinders and braces, the exact values on the weld toe are never used. The value of stress in the zone outside of the influence of the connection geometry but inside the zone of the stress gradient, caused by the geometric effect of the connection is used, and it is extrapolated at the specific point of the weld toe. Thus, referring to the figure below, the design stress is the maximum geometrical peak stress and not the asymptotic value exactly at the connection. [3]

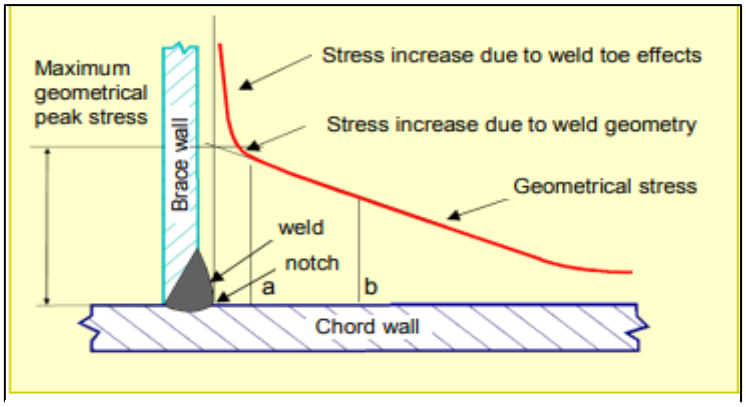

Figure 48. Stress distribution around a weld toe. The exact peak stress at the connection is not used. Instead, geometrical stress or hot spot stress is used.[3]

Despite mentioned before it is stated again for the shake of completeness, that the specific analysis is a multiscale structural mechanics problem. All the above results describe the global response of the structure. Despite being such a large-scale structure, failure would occur at the vicinity of the connections between braces and cylinders which is a very specific region of the structure. Thus, there is also a local scale of the problem that contains those specific regions. Due to the complexity of the problem, it is very hard to ensure satisfactory results in global and local scale at the same time. That's why the formation of a local model is necessary. The global response of the system is fundamental for the development of the local model, since the boundary conditions of the local problem will be the equivalent loads that will be extracted from the stress distribution on the same regions of the global model. The constant focusing on the enhancement of the stress field near the critical regions of the structure is justified, since its essential to make a more effective transition from the global model to the local. That way, more reliable information about the possible failure mechanisms could be obtained and the appropriate redesign to ensure that the structure will have the desired durability, could be implemented more directly. This will be part of the future work presented in chapter 6.

5 Conclusions

Starting from a basic numerical model of the REFOS platform, developed during the execution of the project and implementing a structural model enhancement, especially in terms of computational efficiency, an improved version was eventually obtained. Refining the finite element mesh of the structure and performing a

continuous troubleshooting at different aspects of the model, the following targets were achieved.

- Computational efficiency was substantially ameliorated. To have a quantitative example, the specific simulation of REFOS platform with the improved numerical model, requires only 60-90 minutes of computation time.
- Smoother mesh transitions were developed in critical regions, while the shape of finite elements was improved. The final mesh includes elements with the optimum shape and almost zero distortion ratio.
- An effective remeshing process was established so that denser mesh is applied to the critical regions and coarser mesh on the less critical areas. That gave the appropriate flexibility to the model, since it gives more detailed results at critical areas, while experiencing relatively low computational cost.
- The remeshing on the critical regions of the structure, improved the global response of the system and makes the transition from the global to the local model more effective.

Considering again the large dimensions of the platform depicted at Figure 3 one can realize that the only way to conduct real experiments is to develop a sufficiently scaled down model. Prior to that though, the development of a reliable numerical model that could predict the global response of the structure to a variety of different load cases, especially for such large-scale structures, is crucial. As mentioned before, the effective calculation of the stress field around the critical regions of the structure is appropriate to make the transition from the global to the local scale. Working on the local scale, different configurations at the critical regions could be developed and tested more directly, until the desired results are obtained. The development of such model is a powerful tool for structural optimization and redesign, which is the ultimate target of the project. In the context of the current thesis, the most demanding part of the procedure, was the process of troubleshooting, required to obtain the desired computational efficiency for the global model, has been achieved. To investigate the possible failure mechanisms on the critical points of the structure and be able to have an estimation about the strength of the platform, the transition from the global to the local model is essential. This will be the main context of the future work.

The loads of the structure describe the extreme condition and there is a possibility that plastic strain could occur at specific regions of the structure. Therefore, to make a more realistic analysis, elastic-plastic analysis could be implemented instead of elastic. In the following chapter an approach to implement elastic-plastic analysis is described.

The overall target of REFOS project involves the structural and economic feasibility of the platform. Therefore, improvement of the initial design in terms of geometry, as well as reduction of the total weight of the platform in terms of fabrication cost are proposed. The above ideas are contained in the future work chapter, but their implementation will be straightforward given the fact that an efficient numerical model that effectively describes the global response of the system is now available.

6 Future Work/Ideas

So far, the major outcome of this 'numerical model optimization' procedure was the improvement in computational efficiency. To predict more effectively the response of the critical regions of the structure, and thus investigate further the local failure mechanisms that could occur, a new model focusing on those specific regions must be formed. Despite having a global response of the system, only the critical regions will determine the strength and the life cycle of the total platform. Therefore, the design of a scaled down model is a major asset future work. Subsequently, to achieve a more realistic behavior, especially for the surfaces of the model that carry the greater loads, elastic-plastic analysis should be performed.

6.1 Design of a local finite element model that includes only the areas of most interest.

Since the transition from the global scale to the local scale is critical for the accurate depiction of stress field around the critical regions of the structure, a local model that will contain only those regions should be created. This could be done for all connections between cylinders and braces, but it would be more beneficial if the most demanding connections will be modeled which are those on the central cylinder. The method to develop the local scale model, is to extract the stress field values from the vicinity of the critical region that will be used as boundary conditions of the local model. That way the analysis will be focused on the most interesting locations. A major benefit is the ability to manipulate the selected area and make changes in mesh quality without having to simulate the whole model response. Thus, the results will be obtained in less time. Furthermore, since the simulation would last only several minutes, structural optimization becomes more straightforward, as new design ideas could be tested immediately without severe computational cost. The analysis in the local scale would yield in a more effective prediction of structure's life cycle.

Besides the development of the local numerical model, the equivalent loads that emerge from the stress field of global response of the system, could be used to conduct a scaled down laboratory physical experiment at a specific connection on the central cylinder of the structure. That way, we could compute the strains and estimate the stresses in the laboratory and compare with the results from the corresponding numerical analysis.

6.2 Elastic-Plastic Analysis

All the simulations conducted with the present model, assumed only the elastic response of the system. This is the main reason why at the points that geometrical discontinuities exist, unbounded stress values occur. The implementation of elastic-plastic analysis, by providing to ABAQUS solver information about the plastic response of the steel material, will limit those values to a realistic level. Apart from that issue though, since the simulation of the platform is performed against the extreme loading case scenario, there is the possibility that some points of the structure will undergo plastic deformation. Thus, the elastic-plastic analysis will result in more reliable and realistic stress distribution, at those specific regions.

A set of new ideas and alterations of the current geometry that could hopefully optimize further the global structural response of the structure would be beneficial for the sustainability of the project. Specific adjustments have been proposed which are analyzed further below.

6.3 Brace Connection

An improvement in geometry of the structure has been proposed and that includes extending the braces that connect the circumferential cylinders to the central one and forming a Y-connection inside the central cylinder. The existing design and the addition of the extension of braces is illustrated in Figure 49. This change in the design may be crucial, aiming at relieving the high stress concentration factors that occur in the connections between braces and central cylinder. In this case, the structural strength of the connection may be higher during the operational period of the WT.

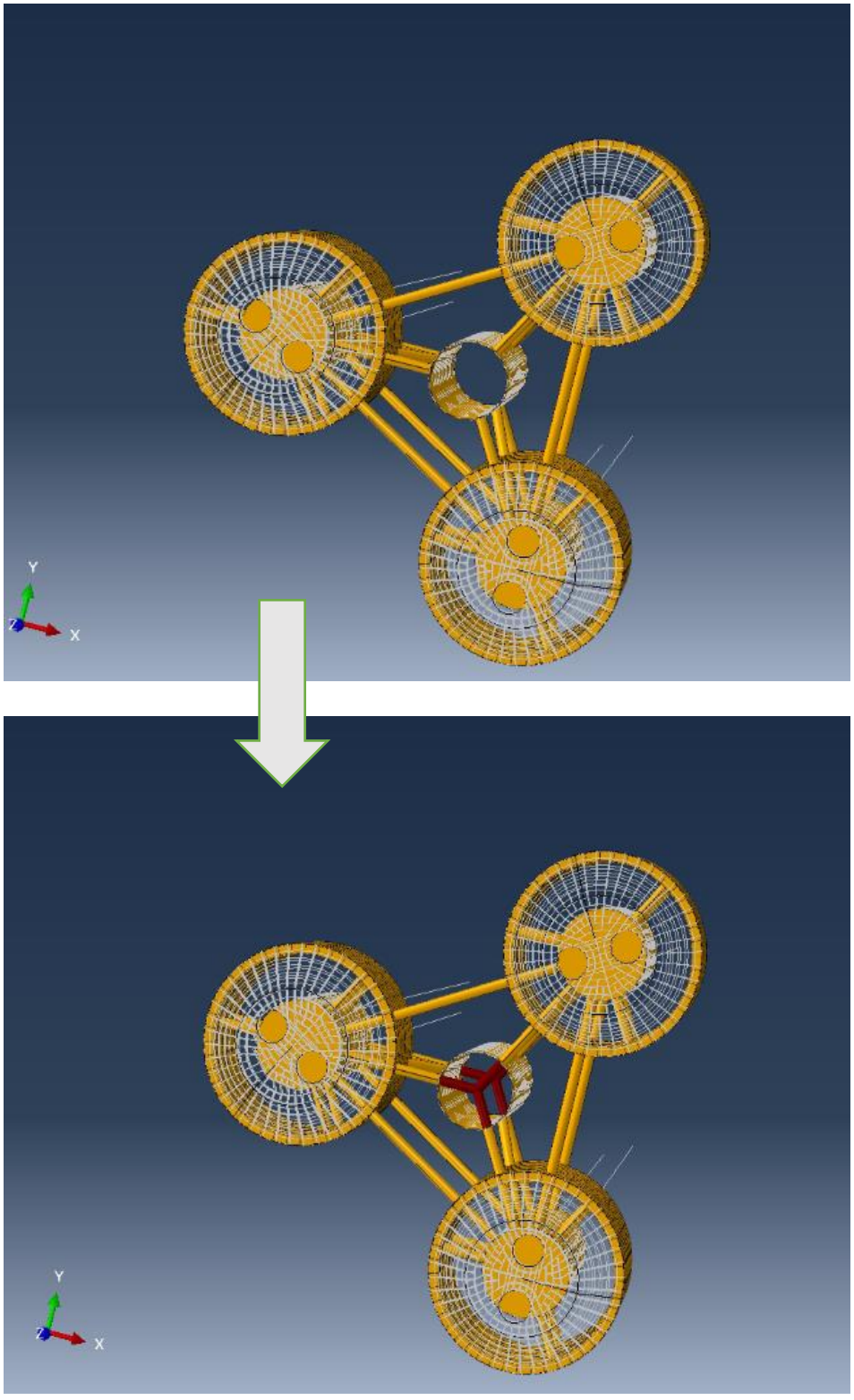

Figure 49. Platform with the current design (top picture) compared to the platform with the extension of braces (bottom picture).

6.4 Model without OWCs.

OWCs while important to produce wave energy, they make the structure heavier and more expensive to construct. In REFOS project it has been shown that they improve the energy output of the system by producing wave energy equal about to 6-8% of the wind energy output of the WT. So, a possible idea to be implemented is to simulate the structure without the OWCs. That way, the model will be more cost-efficient as its weight will be significantly reduced. One may argue that, in this new configuration, without OWCs, the structure may need a global redesign. But this is out of the scope of the present study. The current structure without OWC devices is illustrated in Figure 50. The total mass of the platform reduces to 5043 tones which is almost the half of the original design's mass. A basic question that arises is if the presence of OWC is a benefit that overcome the deficiencies described above in order to payback the investment used for their construction and operation. On the other hand, removing the OWCs besides decreasing the energy output of the total configuration, it may negatively affect the rigidity of the structure and cause structural instability, since the OWC chambers were protecting the column cylinders from the extreme hydrodynamic loads. Therefore, it is quite important to investigate the possibility of removing the OWCs proposal and answer whether this might be better from a structural and economical point of view.

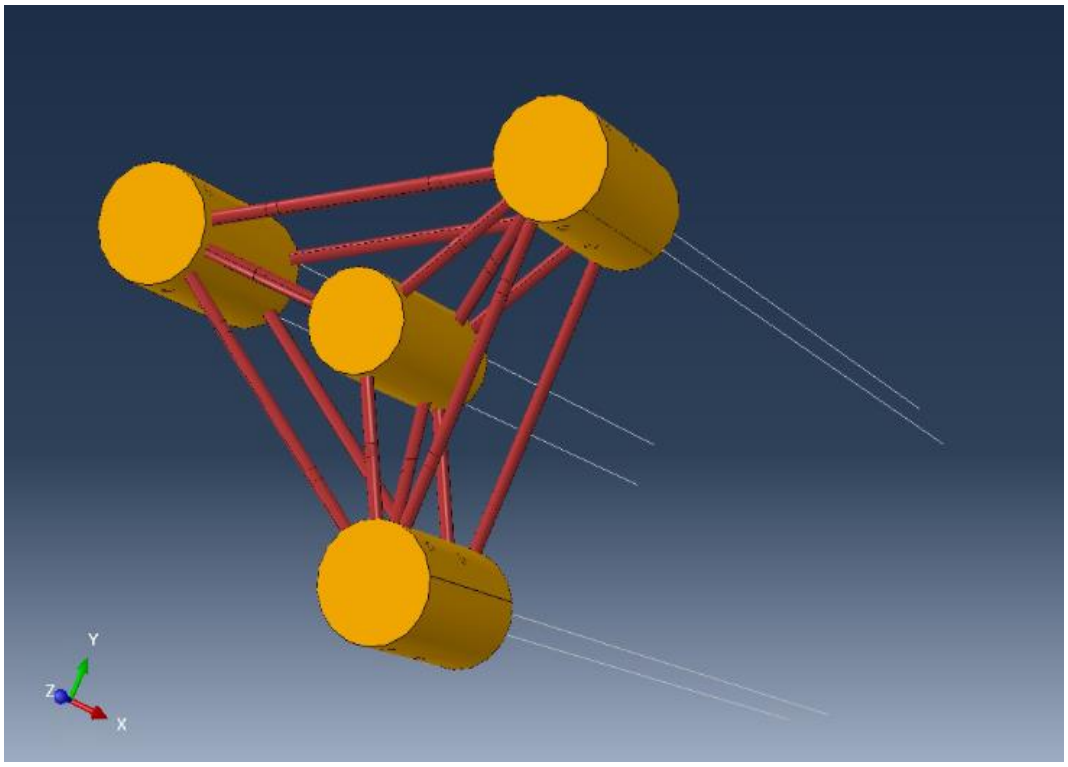

Figure 50. Platform without OWC devices.

6.5 Reduction on thickness of the components of the platform.

A smaller thickness can be applied in specific parts of the model, especially those that are subjected to lower loads. Based on the results of the structural analysis, no significant stress concentration is observed at the OWCs. Thus, a reduction on thickness could be implemented and simulated to examine how that change affects the global response of the system. Furthermore, a thickness reduction could be implemented on the braces. If the emerging stress magnitude is within acceptable range, this solution will result in less material used for braces, reducing significantly the production cost, the weight of the structure and the welding process.

6.6 Fatigue analysis at connections.

The present model can be used for simulating the structure response against multicyclic fatigue. The environmental loads that are exerted to the platform are dynamic and their frequency changes over time. Thus, the platform will be continuously subjected to cyclic loads during its operation. To conduct a fatigue analysis to the structure, both the global(present) model and the local model must be employed. Thus, the global response of the system against multicycle fatigue should initially obtained and subsequently the equivalent loads for the critical regions of the structure need to be calculated. The fatigue life of the total structure depends primarily on the fatigue life of connections between cylinder and braces. Thus, the fatigue life of connections should be higher than 20-year design life of the wind turbine. In case that this criterion is not met, redesign should take place.

REFERENCES

[1] ABAQUS Theory Manual
[2] Abaqus Analysis User's Manual
[3] J. Wardenier, J.A. Packer, X.-L. Zhao and G.J. van der Vegte "Hollow sections in structural applications"
[4] James G. Speight Subsea and Deepwater Oil and Gas Science Technology
[5] Konispoliatis, D.N., Mazarakos, T.P., Mavrakos, S.A. 2016. Hydrodynamic analysis of three-unit arrays of floating annular oscillating-water-column wave energy converters. Applied Ocean Research; 61: p. 42-64
[6] Office of Energy Efficiency & Renewable Energy
[7] Deliverable D1.1-REFOS,2017: State-of-the-art-review
[8] Deliverable D1.3-REFOS,2017: General arrangement of the floating supporting structure with its components and hydrostatic calculations
[9] Deliverable D1.4-REFOS,2017: Dimensioning, operational conditions and loading cases for the W/T
[10] Deliverable D2.4-REFOS,2018: Coupled hydro-aero-elastic behavior of the moored floating multi-purpose platform with OWC's devices and W/T in the time-domain
[11] Deliverable D6.1-REFOS,2018: Report on design of experiments and experimental set up for the scaled-down multi-purpose REFOS floating structure.
[12] Deliverable D4.2-REFOS,2018: Structural design of steel floating supporting structure
[13] Deliverable D7.2-REFOS,2019: Report with the final design of steel tubular platform
[14] Deliverable D7.3-REFOS 2019: Design of the steel tubular TLP tendons